WILEY-VCH

DOI: 10.1002/ ((please add manuscript number))
Article type: Feature Article

Title: Predicting the self-assembly of superparamagnetic colloids under magnetic fields

Jordi Faraudo, Jordi Andreu, Carles Calero and Juan Camacho*

Dr J. Faraudo, Dr J.S. Andreu
Institut de Ciència de Materials de Barcelona (ICMAB-CSIC), C/ dels Til·lers s/n, Campus UAB, E-08193
Bellaterra, Spain.
E-mail: jfaraudo@icmab.es

Dr C. Calero
Dept. de Física Fonamental, Facultat de Física, Universitat de Barcelona
C/Martí i Franquès, 1, E-08028 Barcelona, Spain

Dr. J. Camacho
Dept. de Física, Universitat Autònoma de Barcelona, Campus UAB, E-08193
Bellaterra, Spain

Keywords: magnetic field directed self-assembly, superparamagnetism, colloidal materials, thermodynamics of self-assembly, theory and simulation

Abstract

Self-assembly processes are very important in Material Sciences but are particularly difficult to predict quantitatively. This is the case for particulate magnetic materials; in which field induced self-assembly processes are essential. This Feature Article describes the recent advances in the development of predictive theoretical tools for the study of directed self-assembly of superparamagnetic colloids under magnetic fields. A practical view is presented of how to employ the new concepts (derived from thermodynamic theory) to predict the possible assembled structures from the properties of the colloids and thermodynamic conditions. Quantitative prediction of kinetics is also discussed for the cases in which equilibrium theory is not relevant. Finally, an outline of fundamental aspects of the theory is presented.

1. Introduction

Superparamagnetism[1–3] is a peculiar magnetic behavior observed in small nanoparticles of ferromagnetic materials (such as iron oxide) and in composites containing these nanoparticles. At a first look, superparamagnetism is somehow reminiscent of classical Langevin paramagnetism but with an exceptionally strong magnetic response to an external magnetic field with a high saturation magnetization (hence the prefix "super" in the name). Superparamagnetic materials do not present magnetic hysteresis and, in the absence of external magnetic field, the magnetization of a superparamagnetic material is zero; they do not have remanent magnetization. Therefore, they can be easily manipulated by applied magnetic fields. This highly tunable behavior makes these materials highly attractive for many applications[4,5]. These applications are extremely diverse and include: ferrofluids[6,7] used as sealants or lubricants; multifunctional materials such as reconfigurable coatings[8] or magnetically controllable photonic colloidal crystals[9,10]; materials for biological and biomedical applications[11–14] such as immunoassays, drug delivery or hyperthermia treatments; adsorbent materials for magnetic separation[15–17] or magnetic actuators[18] for microfluidics. Many of these applications employ superparamagnetic particles in the form of composite superparamagnetic colloids. These are composite particles of typical size in the range 50 nm -2 μm made of a nonmagnetic matrix (for example polymer[19] or silica[20]) which contain a large number of superparamagnetic nanocrystals of sizes of a few nanometers inside. In addition to the superparamagnetic property, further functionalities can be added to the colloid either by choosing an appropriate nonmagnetic matrix or by attaching specific ligands to the surface of the colloidal particle. For example, in Ref[21] a carbohydrate matrix with high sorption capacity for metal ions was employed to develop advanced materials for the removal of metal ions using magnetic fields. In Refs[22,23] luminescent functionalities

were added to magnetic colloids by adding quantum dots to the matrix. For biotechnological applications such as protein purification, the preferred strategy is the addition of appropriate ligands to the colloid surface[11].

In the presence of an applied field, these superparamagnetic colloidal particles can self-assembly in a variety of anisotropic structures such as chains of particles, bundles of chains of particles in zippered configurations and fibrous structures made of bundles of chains. For example, in Refs[24–27] the authors employed optical microscopy to observe the behavior of composite superparamagnetic colloids of sizes between 500 nm -800 nm under magnetic fields. In these experiments, it was observed that the particles assembled into linear chains after applying a magnetic field. Interestingly, the chains disappeared (the particles spontaneously re-disperse) after the removal of the external magnetic field[25,27]. Experiments also show that long chains can interact laterally and coalesce in a zippering configuration[28–30] , giving rise to thick chains. Also, more complex, fibrous structures containing bundles of chains can be obtained[31].

The formation of these anisotropic structures is essential in certain applications but is detrimental in other applications. In nanofabrication applications[32] and in responsive materials[8], assembly is essential. Another example in which assembly is essential is magnetophoresis[16] (the transport of magnetic particles induced by a magnetic gradient), which is the principle behind the magnetic separation step[15,17] in applications such as protein purification or pollutant removal. We have shown that the formation of field-induced structures dramatically enhances magnetophoretic velocity[31,33,34].

However, in certain applications the formation of these structures should be avoided. In biomedical applications, assembly is often an undesired effect because the formation of aggregates often reduces biocompatibility. In other cases, field-induced assembly is undesired because it introduces an aging or time dependence in properties which need to be stationary for the applications. For example, in the case of superparamagnetic particles employed as

contrast agents in MRI, the transversal (T_2) relaxation time (which is one of the properties of interest) changes with time if the magnetic interaction between particles induced by the external field is strong enough to give rise to the formation of chains of particles[35–37]. The formation of linear aggregates also has important consequences in hyperthermia applications of superparamagnetic particles[38].

It is therefore highly desirable to anticipate or predict the self-assembly behavior of these materials under magnetic fields from the very beginning of the design of the materials, in order to obtain better materials with the desired behavior. In this respect, theoretical methods, in the form of analytical equations or computational tools could be very helpful. In this Feature Article we will discuss the concepts and methods developed in the last years, suitable for the prediction of the behavior of composite superparamagnetic colloids under magnetic fields. Particular emphasis will be made on how to obtain useful predictions of assembly processes from basic characterization data of the building blocks (size and magnetic response of the particles) and experimental conditions (concentration, temperature). We will discuss simple analytical mathematical formulas for the assembled equilibrium state derived from mean-field, thermodynamic theory[34,39] formally similar to the popular theories employed in the field of supramolecular self-assembly[40]. The prediction of the kinetics will be also discussed, particularly for the cases in which equilibrium thermodynamic theory is not relevant. As we will see, prediction of kinetics requires the use of especially designed computational techniques, introduced to deal with the multiple time and length scales present in the assembly processes of superparamagnetic particles under magnetic fields. In all the cases we will discuss explicitly relevant experimental examples.

The paper is organized as follows. In Section 2, we will present the basic concepts of superparamagnetic colloids and how to model it. In Section 3 we will present the main results from the equilibrium thermodynamic theory, focusing our discussion on practical aspects, emphasizing how to apply the basic concepts. In Section 4, we will discuss how to obtain

kinetic predictions for the cases in which equilibrium thermodynamic theory discussed in the previous sections is not relevant. Section 5 will be devoted to fundamental aspects, discussing the foundations of the thermodynamic self-assembly theory presented in Section 2 as well as comparison with previous theories. We will end up with a Conclusions section.

2. **What are superparamagnetic colloids and how to model them**?

A brief digression on the origin of superparamagnetism is important before discussing the behavior of composite superparamagnetic colloids. The superparamagnetic behavior appears for small nanocrystalls of magnetic materials, as shown schematically in **Figure 1**. Magnetic solids with ferromagnetic or ferrimagnetic behavior contain domains with well-defined size and magnetization, separated by domain walls[2]. Under the effect of a magnetic field, the magnetization of a multidomain sample changes (in response to the applied field) by displacements of the domain wall. The fact that these domains have a characteristic minimum size for each material has very important implications for small particles of magnetic materials. The theory of magnetic domains[1,2] predicts that particles smaller than a certain critical size D_c are monodomain, that is, they are in a state of uniform magnetization both in the absence or in the presence of any external magnetic field (Figure 1). This critical size D_c is different for each material[41], for example it is about 55 nm for FePt but it is as large as 100 nm for $CoFe_2O_4$. This monodomain character has a substantial impact in the magnetic response of the material. For a single domain particle, the "easy" process of wall displacement is not possible and a change in magnetization by an external field requires a more difficult process, namely the rotation of the whole magnetization of the particle. This process has a large energy cost associated to the work against anisotropy energy and, as a consequence, a single domain particle has higher coercitivity than the bulk (multidomain) magnetic material.

For sufficiently small particles (Figure 1), of size D_{sp}, the anisotropy energy can be of the order of the thermal energy. In this situation, the magnetic moment of a single domain particle is thermally unstable and changes spontaneously and rapidly, without applied field. This process of thermal flip of the whole magnetization of the particle is known as Néel relaxation and can be described rigorously by the stochastic theory developed by W.F. Brown[42]. Nanocrystalls have superparamagnetic[3] response when the timescale of the Néel relaxation process, τ_N, is much smaller than the time scale of the magnetic measurements. The observed magnetization is zero in absence of applied field due to the rapid rotation of the single magnetic domain of the particle. In the presence of an applied field, the particles behave as classical, Langevin paramagnets[3] without hysteresis and with a large saturation magnetization (the collective moment of the single domain) which is of the order of 10^4-10^5 times the atomic magnetic moment. The values for D_{sp} are one order of magnitude smaller than the corresponding values of D_{cr} for the same materials. It should be emphasized that the superparamagnetic size D_{sp} of a nanoparticle is usually *defined* as the size at which the Néel relaxation time is τ_N=100 s at ambient temperature. With this definition, one has for example[41], D_{sp}≈10 nm for $CoFe_2O_4$ and D_{sp}≈ 3 nm for FePt.

It is interesting to note that single domain nanoparticles (with sizes larger than D_{sp} but smaller than D_{cr}) can behave effectively as superparamagnetic particles when prepared in liquid suspension as a ferrofluid[7]. In this case, the rotation of the whole particle can be done by the brownian motion of the nanoparticle in solution. Depending on the size of the nanoparticle and the solvent viscosity, the brownian relaxation can be fast, below the time scales of magnetization measurements[43]. Although these particles may behave effectively as superparamagnets, they present some peculiarities. Due to their relatively large size, monodomain particles may have large magnetic dipoles and the dipole-dipole interaction between them could be much larger than the thermal energy. This has important implications.

For example, due to these interactions, monodomain particles in suspension may self-assemble in absence of any external magnetic field[44–48].

Our interest here is in composite materials containing many superparamagnetic nanoparticles (i.e. with size below D_{sp}) in nonmagnetic matrix. More specifically, we are interested in colloidal particles as those described in the Introduction, with sizes in the range 50 nm -2 μm made of a nonmagnetic matrix which contain a large number of superparamagnetic nanocrystals inside. In Figure 1b, we show a typical image[19] of one of these composite colloids and its magnetic response. The composite particle (nonmagnetic matrix with superparamagnetic NPs) has a superparamagnetic response[19,49], provided that the NPs inside the colloid are separated by nonmagnetic material (otherwise, close contact between NPs may induce ferromagnetic behavior[50]). Usually, the NPs inside the colloid are not all identical and in fact, it is possible to derive the size distribution of the NPs inside the colloid from a detailed analysis of its magnetization M=M(H)[49]. In **Figure 1** we illustrate the origin of the magnetic response of the colloid. When H=0, the NPs located inside a colloid have an unstable magnetic moment that freely rotates in all directions due to Neel relaxation.The colloid, which contains a large number of these NPs, has a zero net magnetic moment. For H≠0, the moments of the nanoparticles fluctuate around the direction of the external field. As a result, the colloid has a net magnetization in the direction of the applied field. Under sufficiently strong H fields, the magnetic moments of the NPs become completely aligned to the applied external field and the colloid reaches saturation magnetization. Figure 1c also emphasizes the important point that the model for the behavior of a colloid composed by many NPs is different from the model describing individual NPs. On the one hand, the behavior of single NP is represented by a rapidly rotating magnetic dipole, with an orientation that can be biased by an applied magnetic field. On the other hand, the response of a composite colloid containing many individual superparamagnetic NPs (each one relaxing with the Neel mechanism) can be represented with a magnetic moment *m* which is always aligned

to the external field, with an intensity that increases with the intensity of the applied field and is zero in absence of external field. This representation will be denoted here as the Aligned MacroDipole model (AMD). An interesting consequence of the AMD model is that, in absence of external magnetic field, the composite colloids do not have magnetization (Figure 1) and therefore do not assemble. In order to induce self-assembly, the colloids need to acquire a magnetic moment induced by the external field. Another consequence is that any assembled structure of colloids obtained with an applied magnetic field is observed to disaggregate[27,31,51] when the field is removed (since the magnetic interaction disappears). Colloid-colloid magnetic interactions and their derived self-assembled structures can be completely switched on and off by the applied magnetic field.

In general, the AMD model is valid for any composite spherical particle containing many superparamagnetic NPs in a nonmagnetic matrix. It is important to recall here that the AMD model assumes that the colloid is spherical. In the case of nonspherical colloids (for example, the colloidal triangles obtained in Ref [52]) a single magnetic dipole is not enough to represent the magnetic response of the particle[53], and the model requires extensions that will not be discussed in this paper.

The practical use of the AMD model for predictions requires first a magnetic characterization of the sample which typically gives the magnetization curve per unit mass *M(H)* (measured in Am^2Kg^{-1} or equivalently in emu/g). Then, the magnetic dipolar moment *m(H)* of a colloid of diameter *d* can be computed using:

$$\mathrm{m(H)} = \frac{\pi}{6} d^3 \rho_p \mathrm{M(H)} \qquad (1)$$

where ρ_p is the density of a colloid. As seen in Figure 1b, at low applied fields the magnetic response can be described by a constant magnetic susceptibility χ, defined by $\rho_p \mathrm{M(H)} = \chi \mathrm{H}$. For example, in the case of the colloids of Figure 1b, we have $\chi = 0.6$. In this linear response case, the dipole of a colloid is given by:

$$\mathrm{m(H)} = \frac{\pi}{6} d^3 \chi \mathrm{H} \qquad (2)$$

In an external field, two superparamagnetic colloids with magnetic moment *m* have a magnetic interaction which is strongly anisotropic, and depends not only on the particle separation *r* but also on the angle θ between the magnetic field and the line joining the centers of the two dipoles, see **Figure 2**. The magnetic interaction energy is given by ($\mu_0 = 4\pi \times 10^{-7}$ N A^{-2} is the magnetic permeability of free space):

$$U(r,\theta) = -\frac{\mu_0 \mathrm{m}^2}{2\pi r^3}\left[1 - \frac{3}{2}\sin^2\theta\right] = -U^* \frac{\mathrm{d}^3}{\mathrm{r}^3}\left[1 - \frac{3}{2}\sin^2\theta\right] \qquad (3)$$

where U^* is the maximum value of the magnetic energy, given by:

$$U^* = \frac{\mu_0 \mathrm{m}^2}{2\pi d^3} \qquad (4)$$

As shown in Figure 2, the interaction energy given by Equation (3) is attractive ($U<0$) for angles $\theta<54.7°$ and repulsive ($U>0$) for $\theta>54.7°$. The magnetic energy has its minimum value ($-U^*$) for tip-to-tip aligned dipoles in contact ($r=d$ and $\theta=0$) and it has its maximum repulsion ($U=U^*/2$) for two parallel dipoles in contact ($r=d$ and $\theta=90°$). This anisotropic colloid-colloid magnetic interaction tends to induce the formation of anisotropic structures in the direction of the applied field. In the next section we will discuss which structures are found and under which conditions appear.

Before ending the section, a technical point should be noted here regarding the use of Equation (3) and (4) in practical situations. In principle, the magnetic field *H* to be employed in the calculation of the dipole moment $m(H)$ in Equation (1) should be the total field on a colloid, including the external applied field H_0 and the field sensed by a colloid due to the other colloids (induced dipole contribution). However, the induced dipole contribution is usually very small and we can safely approximate the field over a particle to the external field $\mathrm{H} \approx \mathrm{H}_0$ in Equation (1) except possibly in the case of weak external fields. The induced dipole contribution can be easily estimated in the linear response region in which the magnetization

of the colloid is characterized by the susceptibility χ (see Equation (2)). Considering a dimer of two particles in contact in the most favorable orientation (θ=0), the magnetization of a particle is given by[54] (see also the Supporting Information for details):

$$m(H) = \frac{\pi}{6} d^3 \chi H = \frac{\pi}{6} d^3 \left[1 - \frac{\chi}{12}\right]^{-1} \chi H_0 \quad (5)$$

where the factor in parenthesis is the induced dipole correction. This correction implies only a modest increment in the magnetic dipole (only a 5% for χ=0.6 for example) as compared with that expected considering only the applied field H_0.

3. **Basic principles of field-induced self-assembly of Superparamagnetic colloids**

Once we have formulated a model for superparamagnetic colloids (AMD model, Figures 1 and 2), we discuss its predictions. In this section we will summarize the most important predictions from the model, in the form of self-assembly rules. We will illustrate their use comparing with published results from experiments and computer simulations.

We argued in the previous section that, in the presence of a magnetic field, the magnetic interaction between colloids may induce the formation of anisotropic structures. But the conditions for the formation of the structures depend not only on magnetic energy considerations but also on thermodynamic considerations. The reason is that in a colloidal dispersion one has to take into account not only the energy decrease involved in the formation of a magnetic association but also the loss of entropy in the solution associated with the formation of structures of different sizes. A thermodynamic analysis[34,39] (see also Section 5 for a detailed derivation) shows that the balance between energetic and entropic factors is determined by a dimensionless quantity, the so-called aggregation parameter N^*, which involves not only the magnetic properties of the colloids but also thermodynamic variables such as concentration and temperature. The critical value of N^* for field-induced self-assembly is $N^*=1$. In the case of $N^*<1$, the formation of structures is not possible (entropy

dominates) whereas for $N^*>1$, the particles will form different kinds of elongated structures (chains or bundles of chains), as depicted schematically in **Figure 3**. This aggregation parameter N^* can be computed from the properties of the suspension by:

$$N^* = \sqrt{\phi_0 e^{\Gamma-1}} \tag{6}$$

where ϕ_0 is the volume fraction of the suspension occupied by colloids and Γ is the magnetic coupling parameter:

$$\phi_0 = \frac{\pi}{6} d^3 n = \frac{\pi}{6} d^3 \frac{c}{\rho_p} \tag{7}$$

$$\Gamma = \frac{\mu_0 \mathrm{m}^2}{2\pi d^3 k_B T} \tag{8}$$

In Equation (7), n is the number of colloids per unit volume and c its mass concentration (mass of particles per unit volume). The magnetic coupling parameter Γ defined in Equation (8) is simply the ratio between the maximum value for the attractive magnetic energy U^* (Equation (4)) and the thermal energy k_BT (k_B=1.38×10^{-23} JK^{-1} is the Boltzmann constant, T is the absolute temperature). In Table 1 we have collected representative values of the parameters ϕ_0, Γ and N^* calculated in experiments with superparamagnetic colloids (in all cases, the experiments were done under strong fields, so we employed the magnetic moment corresponding to saturation magnetization in Equation (1)).

Before discussing in more detail the predictions of the theory with particular examples, let us briefly discuss a few direct implications of Equation (6), (7) and (8). Of course, if thermal agitation is stronger than magnetic interaction ($\Gamma<1$) we will have $N^*<1$ and no field-induced self-assembly will occur. Values of Γ larger than 1 imply that the magnetic interaction between particles in contact is stronger than thermal energy, but self-assembly is not guaranteed. According to Equation (6), the actual condition determining the formation of structures ($N^*>1$) involves not only Γ but also the volume fraction ϕ_0. Both experiments[33] and simulations[39] show examples of situations with $\Gamma>1$ in which no field-induced self-

assembly was observed. Dispersions of superparamagnetic colloids rarely exceed 5% in volume (ϕ_0=0.05), so Equation (6) implies that particles with Γ<4 will not experience self-assembly under the effect of a magnetic field in spite of their substantial magnetic response. In applications in which field-induced self-assembly is undesired one has to work in conditions of Γ<4, otherwise the concentration of the suspension should be carefully controlled to be low enough in order to guarantee that N^* is still below 1. On the contrary, assembly of particles (N^*>1) will be unavoidable for particles with Γ>15, even in extremely diluted conditions, since the smaller volume fractions reported in experiments[35] are of the order of $\phi_0 \approx 10^{-6}$.

We will discuss now in more detail the different possibilities shown in Figure 3. Let us consider first the case N^* <1. According to our theory, in this case there cannot be formation of structures. These predictions can be compared with the experimental observations corresponding to samples S1-S3 in Table 1, which are superparamagnetic colloids proposed for use as contrast agents in magnetic resonance imaging (MRI) applications (see Refs[20,55]). In these cases, one typically employs strong magnetic fields and the particles are near magnetic saturation. A large magnetic response of the particles is desired but field-induced self-assembly is unwanted for these applications. As it can be seen in Table 1, all these samples (S1-S3) have values of N*<1, corresponding to no formation of structures. In all three cases, magnetophoresis measurements[33,55] clearly show the absence of chain formation, in agreement with our prediction. It is interesting to note that in the cases of S2 and S3 there is no self-assembly (entropy "wins", N*<1) in spite of the presence of particle-particle magnetic interactions stronger than thermal energy (Γ>1). In the case of S3, we predict that formation of chains will be possible by performing new experiments at larger concentration. According to Equation (6) and the data in Table 1, one needs a volume fraction larger than 10^{-3} in order

to obtain chains, which is a substantial increase over the diluted concentration employed in experiments in Ref[55], but it is a feasible concentration.

In the case of N^*>1, we will observe magnetic field induced self-assembly of the particles, as shown schematically in Figure 3. For moderate values of N^*, (N^* <10) the equilibrium state of the colloidal dispersion consists of chains of different sizes, with a probability of finding a chain containing l particles given by $\boldsymbol{p} \propto \mathbf{exp}(-\frac{\boldsymbol{l}}{\boldsymbol{N^*}})$. The average number of particles in a chain (its average length) is given by:

$$< l > \approx N^* \qquad (N^* > 1) \tag{9}$$

For values of N^* >10, the equilibrium state consist of chains and also thicker structures made by self-assembly of long chains. These are bundles of zippered chains in which particles in neighboring chains are organized out of registry by a distance of $d/2$, as shown in Figure 3c. The reason for these structures is due to the peculiar behavior of magnetic interactions between long chains (see section 5 and also Ref[56] for more details). Chains longer than a certain critical value (14 particles) can aggregate laterally to form thicker aggregates (bundles of chains). This effect is relevant as long as there is a substantial fraction of chains longer than this critical value, which occurs for N^*>10. In this case of bundle formation the average length of the aggregates in the system can still approximately calculated using Equation (9). However, we are not aware of analytical equations to estimate the number of chains per bundle or the average number of particles per bundle.

These predictions can also be compared with experimental results and computer simulations. A systematic comparison with computer simulations is summarized in Table 2 for different values of N^* either by considering different concentrations (i.e. different ϕ_0) at a given Γ or different values of the magnetic coupling parameter Γ at a given ϕ_0. As seen in Table 2, the average length of the chains obtained in simulations is in very good agreement with the prediction from Equation (9). Concerning experiments, we can consider the case of

sample S4 in Table 1, in which NMR experiments[30,57] were employed to follow the field-induced self-assembly process. The experimental results showed a two step aggregation process, corresponding to a first step with the formation of chains and a second step (at larger times) corresponding to the formation of bundles of zippered chains. This behavior is in complete agreement with that expected from the estimated value of N^* ($N^* \approx 24$), see Figure 3. Unfortunately, from the experimental results it was not possible to estimate the sizes of the structures, but computer simulations of the experimental system[57] (simulation S7 in Table 2) showed that the average length of the chains (including bundles of chains and single chains) is about 25 particles, in excellent agreement with the prediction of Equation (9).

Finally, let us consider the case of very large values of N^*. As it can be seen in Table 1 (samples S5 and S6 from Refs[35,37,58]), there are situations in which the magnetic coupling parameter can be very large ($\Gamma > 100$). Due to the exponential dependence of N^* with Γ (see Equation (4)), this case corresponds to extremely large –almost divergent– values of N^*. In this case, magnetic interaction dominates over entropic factors and the equilibrium state is dictated purely by considerations of minimum magnetic energy. The minimum energy state corresponds to a collapse of the system in the form of an extremely large bundle which contains all the particles of the system. However, we cannot expect to be able to observe this state, as it will require an extremely large observation time (see discussion in Ref[39]). At the experimental time scales, we will observe the formation of chains and bundles of chains which will continue growing without reaching an equilibrium state. As examples of this case, let us consider samples S5 and S6 in Table 1. In the case of sample S5, NMR experiments were performed to measure the transversal relaxation time T_2 of water protons, which provides an indirect way to estimate the size of the field-induced aggregates. The magnetic coupling was very high in this case ($\Gamma = 247$) but the experiments were performed at very low concentrations (10^{-6}-10^{-5}) in order to check whether a very low concentration can prevent

self-assembly even for strongly magnetic particles. In spite of the low concentration, the experimental results clearly indicated the formation of chains, which were continuously growing during the experiments, as expected from our previous theoretical considerations. The kinetics of the process, which was observed in detail in this case, will be discussed in the next subsection as compared with predictions from computer simulations. The case of sample S6 in Table 1 (Ref[37]) corresponds to a situation with an even larger magnetic coupling parameter ($\Gamma \approx 400$). In this case, the structures obtained at different times were observed with dark field microscopy. The observations corroborate again the expectations from the theory. At short times, the formation of chains was observed and at longer times formation of bundles of chains was observed. The observed bundles corresponded to chains of lengths larger than the critical value (14 particles) predicted theoretically.

Up to now, we have employed the self-assembly theory for the case of reasonably monodisperse colloids (i.e. a well-defined average size and a low polydispersity index). However, there are situations of interest in which one has at least two clearly different particles (of different size or with different magnetic properties). The theory can be also generalized to this case, although the resulting equations are more complex. However, there is a particular case of interest in which it is possible to find simple analytical solutions. This is the case in which we have strongly magnetic colloids (let us say type "A" particles) with a strong tendency to form chains and weakly magnetic particles (let us say type "B" particles) which do not form chains. The question is under which conditions a mixture of A and B particles will assemble into chains containing both A and B particles or into separated phases with chains of A particles and isolated B particles. To analyze this question, we will need to consider the magnetic coupling parameters Γ_A and Γ_B calculated from Equation (8) for particles of type A and B and their corresponding aggregation numbers N_A^* , N_B^* calculated using Equation (4) with the volume fraction of particles of type A and B respectively. In the case of $N_A^*>1$ and $N_B^*<1$, we have the possibility of chains made exclusively of A particles

and chains containing both A and B particles. The equilibrium ratio f between particles of type B in mixed chains (containing both A and B particles) and free, isolated B particles is given by:

$$f = 2N_A^* \exp\left(\sqrt{\Gamma_A \cdot \Gamma_B} - \Gamma_A\right) = 2\sqrt{\phi_A} \exp\left(\sqrt{\Gamma_A \cdot \Gamma_B} - \frac{1}{2}\Gamma_A - \frac{1}{2}\right). \quad (10)$$

Equation (10) is derived assuming that both types of particles have the same size but different magnetic behaviour (for different sizes, the equations become more involved and are not discussed here for simplicity). Equation (10) implies that the formation of mixed chains is negligible in the cases of $\Gamma_A \gg 1$ and or $\Gamma_B < 1$. In order to find a nonnegligible amount of mixed chains (let us say f larger than 1%) without observing chains made of only B particles, we need to consider not too weakly magnetic B particles ($\Gamma_B < 4$) and not too strongly magnetic A particles ($\Gamma_A < 20$) at high enough concentrations ($\phi_A > 10^{-3}$). This conclusion derived from Equation (10) has interesting implications. For example, as a result of the synthesis process, in Ref[59] the authors obtain a mixture of two kinds of superparamagnetic particles with two very different magnetic response. From their data, we estimate that the more magnetic particles have $\Gamma_A > 10$ and the less magnetic particles have $\Gamma_B < 1$. Following our results, we predict that the application of a strong magnetic field to the sample will produce the formation of chains and bundles made exclusively by the more magnetic particles, excluding the less magnetic ones. This suggests that a separation of the two components of the mixture can be done with the application of a magnetic field, since one kind of particles will be forming large structures whereas the other type of particles will be in the form of small, isolated particles. In Ref[60], the authors indicate that mixtures of particles with very different sizes can be fractionated using magnetophoresis processes. Our results also suggest that a similar magnetophoresis fractionation process can also be possible for particles with very different magnetic responses and similar size.

The discussion in this section shows that the concept of the aggregation parameter N^* and the classification shown in Figure 3 can be extremely useful in the prediction of the magnetic field induced self-assembly of superparamagnetic colloids. Its use is simple, since the parameters contained in the equations can be easily evaluated from the characterization data of the particles.

4. When Equilibrium theory is not enough: predicting kinetics

4.1 Simple kinetic rules

The self-assembly rules described in the previous section correspond to the description of the thermodynamic equilibrium state. It is therefore important to know whether the approach to the equilibrium state is fast (so thermodynamic predictions are relevant) or it is so slow that a description of the kinetics of the self-assembly process instead of a thermodynamic description is needed.

We can distinguish between two main kinetic regimes for superparamagnetic particles under external field: kinetics dominated by the magnetic interaction and kinetics dominated by diffusion. There is a simple rule to determine which mechanism dominates the kinetics. It is based on the comparison between the typical separation between colloidal particles and the particle-particle interaction length scale. Initially (before applying the magnetic field), the distribution of particles is random and the average distance between particles is determined by the concentration. In a random distribution of particles, the average separation between particles d_{pp} is given by the classical Hertz-Chandrasekhar equation[61,62]

$$d_{pp} = 2.7\frac{d}{6\phi_0^{1/3}} \quad . \tag{11}$$

(the numerical prefactor in Equation (11) is the value of the Gamma function[63] evaluated at 1/3). After applying a magnetic field, the colloidal particles will interact due to their magnetic moments induced by the external field, as described in Section 2. In a colloidal dispersion,

this particle-particle interaction will be relevant only for those interparticle distances at which it is stronger than the thermal energy. The ratio between the magnetic interaction energy between two magnetic dipoles *m* and the thermal energy can be obtained from Equation (3) and (7):

$$\frac{U(r,\theta)}{k_B T} = -\Gamma \frac{\mathrm{d}^3}{\mathrm{r}^3}\left[1 - \frac{3}{2}\sin^2\theta\right] = -\frac{\lambda_B^3}{\mathrm{r}^3}\left[1 - \frac{3}{2}\sin^2\theta\right] \qquad (12)$$

In Equation (12) we have introduced the so-called magnetic Bjerrum length[31,34] defined by:

$$\lambda_B = d \cdot \Gamma^{1/3} \quad . \qquad (13)$$

From Equation (12) we see that λ_B is the distance at which the energy associated to attractive magnetic interaction between aligned dipoles is equal to the thermal energy, $U(r = \lambda_B, \theta = 0) = -k_B T$. The relation between d_{pp} and λ_B determines the kinetics of the self-assembly process under an external magnetic field. In the case of $\lambda_B \gg d_{pp}$, the motion of the particles is deterministic, dominated by the magnetic interaction. In the opposite case of $\lambda_B \ll d_{pp}$, the motion of the particles is essentially diffusive and a colloid only feels the magnetic interaction with another particle after randomly diffusing across the distance separating both colloids. In practice, one typically chooses to work in conditions corresponding to one of these two extreme situations, depending on the specific application for which the particles are designed. For applications requiring fast self-assembly one should work in conditions $\lambda_B \gg d_{pp}$, whereas the case $\lambda_B \ll d_{pp}$ is preferred in situations in which self-assembly should be minimized at experimental time scales. Combining Equations (11) and (13), we can also write the conditions involving d_{pp} and λ_B in terms of ϕ_0 and Γ:

$\Gamma\phi_0 \gg 0.1$ deterministic kinetics . (14)

$\Gamma\phi_0 \ll 0.1$ diffusive kinetics. (15)

We can also derive simple, approximate equations for the time scale of the self-assembly process in these two limiting cases. In the limit of kinetics dominated by magnetic

interactions (Equation (14)), the characteristic time t_m needed for aggregation of two particles initially separated by a distance d_{pp} can be estimated by balancing the viscous drag with the magnetic force. The result is approximately given by[56]:

$$t_m \approx \frac{d_{pp}^5 - d^5}{15 D \lambda_B^3} \quad (16)$$

In the opposite case of kinetics dominated by diffusion (Equation (15)), the characteristic time t_B can be roughly estimated by[24] :

$$t_B = \frac{d^2}{48\left[\frac{1}{3^{1/2}} - \frac{1}{3^{3/2}}\right] D \Gamma \phi_0}. \quad (17)$$

Equation (17) was obtained by considering the classical Smoluchowsky rate of aggregation of Brownian spheres adsorbing spheres, with a geometrical modification to account for the region in which magnetic interactions dominate.

We can consider now explicit examples of the two situations. Let us consider first a case in which fast aggregation is highly desired. This is the case for superparamagnetic particles designed for applications involving magnetophoresis (such as immunoessays[19] or removal of pollutants[21]). In this case, the magnetic field is applied for removal of the particles once they have performed their function (e.g. capture of proteins or pollutants). Their magnetophoretic motion is known to be much faster for self-assembled bundles than for isolated particles[31,34], so fast self-assembly is required in order to speed up the whole process. Typical commercial superparamagnetic colloids for use in magnetophoretic separation have very large values of λ_B (of the order of several μm) due to values of the magnetic coupling parameter of the order of $\Gamma \sim 10^3$ (see Refs[31,33]) or even larger[18]. According to Equation (14) the self-assembly process will be dominated by deterministic magnetic interactions for volume fractions larger than 10^{-4}. For example, consider one of the samples reported in Ref[31] consisting of a 1 g/L dispersion (volume fraction 9×10^{-4}) of particles of 200 nm, density 1.1 g/cm^3 and $\Gamma \approx 10^3$. From Equation (11), (12) and (16) we estimate d_{pp}=925 nm, $\lambda_B \approx 2$ μm

and an initial aggregation time due to magnetic forces of $t_m \approx 2\times10^{-3}$ s. Therefore, the formation of field-induced self-assembled structures is very fast at the time scales relevant in magnetophoretic separation processes, which occur at scales of the order of several seconds or minutes.

As an example of the opposite case (self-assembly kinetics dominated by diffusion), let us consider the particles of the case S5 in Table 1, which were designed for use as contrast agents in magnetic resonance imaging. As discussed in the previous subsection, in this case a large magnetic response of the particles is desired, but self-assembly is an undesired effect which is minimized by using very low concentrations. These particles have a large value of the magnetic coupling parameter (Γ=247) and a typical volume fraction was 10^{-5}, so we have $\Gamma\phi_0 \approx 2.5 \times 10^{-3} \ll 0.1$. According to Equation (15) we will have always a diffusive behavior, which is compatible with the very slow kinetics observed experimentally[35]. Using Equation (13) and (11) we obtain for the characteristic length scales of the system $\lambda_B = 0.55$ μm (about 6 times the size of the particles) and d_{pp} ≈1.8 μm (about 21 times the size of the particles), so we have $d_{pp} \gg \lambda_B$. For these particles, we estimated[36] a diffusion coefficient of D≈7.5 μm^2/s, so Equation (17) gives a characteristic time of self-assembly of $t_B \approx 2$ s. At these time scales, the formation of chains begins to be significant, with an average size of chains of about 2 particles[36]. It is interesting to note that in this particular example we have kinetics dominated by diffusion but we have an extremely large value of the aggregation parameter, $N^*\sim10^{52}>>1$, which implies an eventual collapse of the system into a single aggregated structure. In any case, this equilibrium state is not physically relevant, since it will be unreachable under experimental time scales due to the slow kinetics of the aggregation process.

The study of the kinetics has been the subject of many experimental studies in this regime where kinetics is dominated by diffusion ($\Gamma\phi_0 \ll 0.1$), since the slow kinetics makes

possible to follow the different steps of self-assembly in detail using many experimental techniques. We will now discuss some of the results for this case.

4.2 **A brief perspective of results in the case of kinetics dominated by diffusion**

As we mentioned before, there are many experimental techniques suitable for the study of the kinetics of self-assembly in the case $\Gamma\phi_0 \ll 0.1$. A popular approach is to employ in-situ optical microscopy[24,25,64–66] and determine the size and number of chains by direct counting from images taken at different times, using the appropriate image processing software. Another possibility is to follow the assembly process by dynamic light scattering (DLS). In this case, one obtains an effective diffusion coefficient that decreases as a function of time[67,68] that can be employed to evaluate an effective value for the average chain length. More recently, several works[30,35,57] have employed nuclear magnetic resonance (NMR), owing to the fact that the response of the water protons responsible for the NMR signal is very sensitive to local magnetic fields and therefore it is very sensitive to the formation of chains of superparamagnetic colloids.

As a general result from these studies, it has been observed that the kinetics of chain growth follows, for long times, a power law evolution for the average length $< l > \propto t^z$. This power law has been observed to hold in many experimental studies[24,64,65,67,68], although we should emphasize that the numerical value of z is not universal. Most experimental results[24,67,68] are consistent with a power law with values of z between 0.6 and 0.7 although a few experiments[24,65] also report values of z between 0.4 and 0.5. It seems that the value of z depends on the values of ϕ_0 and Γ, but the exact dependence is still not known.

Since diffusion is the dominant mechanism in these experiments, several authors[24,67,68] tried to collapse the kinetics observed under different conditions (different concentrations or different magnetic responses) onto a universal kinetic curve by rescaling the

experimental time by the characteristic diffusion-aggregation time t_B^* defined in Equation (17). A modification to Equation (17) was also proposed in Ref[68] to account not only for magnetic interactions but also for double layer, electrostatic forces. By plotting the kinetic data as a function of t/t_B^* many different experiments show a similar behavior, although the differences between different experimental conditions were still evident after rescaling (see for example Figure 5, 6 and 7 in Ref[24] or Figure 5 in Ref[67]). This suggests a possible inaccuracy of Equation (17) due to the crude approximations made in its derivation or to the presence of additional (slowest) time scales that become relevant as the self-assembly process advances. Interestingly, the collapse is nearly perfect for the data in Ref[68] in which double layer forces (in addition to magnetic forces) play a substantial role.

A further step in the modeling of the kinetics was to consider Smoluchowsky rate equations[68], which consider the balance of creation and destruction of chains of different sizes. In this approach, the number density of chains of k particles, n_k, obeys:

$$\frac{dn_k}{dt} = \frac{1}{2}\sum_{i+j=k} K_{ij} n_i n_j - n_k \sum_{i=1}^{\infty} K_{ik} n_i \quad . \qquad (18)$$

The first term in Equation (18) accounts for the creation of chains of k particles from smaller chains of sizes i and j described by the constant K_{ij}. The second term corresponds to the destruction of chains of k particles due to the aggregation with other chains of length i described by the constants K_{ik}. Equation (18) is appropriate for large values of Γ since it describes the growth of chains from the aggregation of particles or chains of smaller size but it does not take into account the possibility of spontaneous breaking of chains due to thermal agitation. This possibility can be easily included by adding further terms in Equation (18) as shown in Ref[69].

The main problem of this approach is the need to model the constants K_{ij} of the different possibilities for creation and destruction of clusters of all possible sizes. One possibility, followed in Ref[25] is to obtain experimental data on the time evolution of the

distribution n_k for chains of different sizes and fit the rates K_{ij} using Equation (18). This option has the drawback of having little predictive power but it has the fundamental interest of demonstrating the viability of Equation (18) to describe the self-assembly process. In order to proceed further, a commonly employed approximation[24,25] assumes that the rates K_{ij} are proportional to the diffusion coefficients of chains and that the diffusion coefficient of a chain depends as a power law with the size of the chain, $K_{ij} \propto \left(D_i + D_j\right) \propto (i^{-\gamma} + j^{-\gamma})$ where γ is an exponent to be determined. Using this approximation, it can be shown that Equation (18) implies[24] a power law evolution for the average length $< l > \propto t^z$ with exponent $z=1/(1+\gamma)$. Hydrodynamic arguments suggest that $\gamma \approx 1$, so one expects an exponent $z \approx 0.5$, which is consistent with some experiments but it is smaller than the value obtained in most experiments (which give z between 0.6-0.7 as discussed before).

4.3 **Computer Simulations with standard techniques**

In view of the limitations of the available theoretical approaches, there is the possibility to employ detailed computer simulations. Since we have a model for superparamagnetic colloids (the AMD model presented in Section 2) and the equations of motion of colloids in suspension are known, it has to be, in principle, possible to obtain a numerical prediction of the kinetics for a particular system, given the properties of the sample (magnetic response, applied field and size of the particle) under specified conditions (concentration, temperature, …). A technique suitable for these simulations is Langevin Dynamic Simulations (LD). In LD simulations, one solves the Newton equations of motion for each colloid, taking into account all the forces acting over each colloid: the interaction forces between colloids (not only magnetic interactions but other forces can be included) and the forces due to the interaction of the colloid with the solvent (viscous resistance and thermal noise due to solvent-colloid collisions). This methodology can be thought as a generalization,

at the colloidal scale, of the molecular dynamics simulation (MD) technique widely employed in atomistic modeling of materials. In MD one solves the Newtonian equations of motion of all atoms of the system. In LD, one solves the Newton equations of motion of all colloids in an implicit solvent, including the forces relevant at the colloidal scale. In LD, the diffusive motion typical of colloids arises in a natural way as a result of the interaction of the colloids with the solvent. An advantage of the LD technique is that since it is based in the Newton equations of motion, it is implemented in many of MD standard simulation packages employed in Material Sciences, such as LAMMPS[70].

In a typical LD simulation, one can consider systems between 10^3-10^4 colloids. In these simulations, one starts from an initial configuration (for example random dispersion of colloids) and follows the evolution of the system until a desired time, typically up to 1-10 s. The computational cost of these simulations is very large; obtaining 1 s in the kinetics may require of the order of 10^3 hours of computational time. We employed this technique in Ref [39] to obtain most of the data reported in Table 2 and to study the kinetics for different values of ϕ_0 and Γ. In order to illustrate typical results obtained with this technique, in **Figure 4** we show examples of average kinetic results from four LD simulations. We also show a snapshot from a simulation. These four simulations correspond to the same concentration (ϕ_0=5.23×10^{-4}) and increasing values of Γ (3, 10, 15 and 40). The first case (Γ=3) corresponds to case S1 in Table 2, and it has aggregation parameter N^*<1. Consequently, we do not observe formation of chains (only very short lived dimers which induce small fluctuations in the average chain length that are not visible in the scale of Figure 4). The remaining examples correspond to kinetics dominated by diffusion ($\Gamma\phi_0 \ll 0.1$) but very different values of N^*. For Γ=10 and $N^*\approx 2$ (case S2 in Table 2), the system attains the equilibrium state, consisting of short chains, in about 1 s. Before reaching the equilibrium state, the kinetics can be roughly described with a power law of the form $< l > \propto t^z$ with an exponent $z\approx 0.5$. The situation is very different

when we consider a larger magnetic coupling parameter of Γ=15 corresponding to N^*≈25. In this case, we observe a clear linear growth in the log-log plot of Figure 4, indicating a power law of the form $< l > \propto t^z$ with an exponent z≈0.64. In this case, we cannot perform simulations at time scales long enough to observe the equilibrium state. A simple estimation using the observed kinetics shows that to reach average sizes of the order of 25 particles we will need of the order of 10 s, which implies extending the LD simulations one order of magnitude in time, which requires enormous computational resources. We show also the results for Γ=40, which corresponds to $N^*=6.7\times10^6$. In this case, we also observe power law kinetics $< l > \propto t^z$ with an exponent z≈0.64, again consistent with previous reports discussed before.

These results show that it is possible to obtain relevant results from LD simulations but also illustrate its limitations to attain time scales relevant to the self-assembly process. Other standard simulation techniques, closely related to LD (such as Brownian Dynamics simulations as those performed in Ref[65]) also suffer from similar limitations, which explains why realistic computer simulations of the kinetics of this problem are scarce. In fact, such difficulties are not limited to the problem of magnetic field induced self-assembly of superparamagnetic particles, but it affects the whole field of theoretical predictions in the field of self-assembly in Materials Sciences[71], so it is important to understand the origin of the limitations and the possible solutions.

Conceptually, in self-assembly processes, one starts with building blocks which are initially in a disordered (high entropy) state and should end into an assembled, low entropy state of higher order and complexity. The driving force for the ordering of the system are the interactions between the building blocks, which could be Van der Waals forces, electrostatic or magnetic forces, and other well-known interactions[53]. Therefore, for each particular case, in principle we know all ingredients needed for the prediction: the building blocks involved in

the assembly process (molecules, nanoparticles, colloids,…), the interactions controlling the self-assembly process and the equations of physics governing the behavior of the building blocks taking into account the relevant interactions. The difficulties in the predictions are thus not related to the ignorance of the underlying rules, but rather related to the complexity of the self-assembly process. In self-assembly processes, we have multiple time and length scales (and even multiple energy scales), which correspond to the building blocks and their interactions, and to the intermediate structures which are being assembled by these building blocks. The complexity of the problem relies on the fact that we have interactions that need to be computed at small length and time scales but influence the larger time and length scales corresponding to the assembled structures. In turn, the phenomena occurring at these larger time and length scales influence the small-scale behavior of building blocks. Therefore, in most cases it is simply not possible to run a "brute-force" computer simulation with all the interacting building blocks in an initial random state and to follow the full assembly process, even with the current computer resources and capabilities. Let us illustrate this point by considering the scales involved in a specific example of formation of chains of colloids by self-assembly of superparamagnetic particles under an external magnetic field.

Let us consider again the case of sample S5 in Table 1, discussed before in section 4.1, which corresponds to a diluted system (ϕ=10^{-5}) of superparamagnetic colloids at magnetic saturation (Γ=247) designed for use as contrast agents in magnetic resonance imaging. It can be seen that in this problem coexist very different relevant time scales that make simulation a difficult task. In section 4.1, we identified three relevant length scales of the problem: the size of the particles (88 nm), the length scale of magnetic interactions ($\lambda_B = 552$ nm) and the initial average distance between particles (d_{pp} ≈1.8 μm). In a simulation, we have to simulate the diffusive motion of these particles at length scales l smaller than the size of the colloids, otherwise collisions between colloids will not be correctly simulated. As before, using the

estimated diffusion coefficient of $D \approx 7.5\ \mu m^2/s$, this implies a minimum timescale of the order of $t \approx \frac{d^2}{6D} \approx 10^{-4}$ s. Another relevant time scale in a simulation of the process is the time needed to bring two particles initially separated by a distance d_{pp} to the distance λ_B at which magnetic interactions dominate $t_0 \approx \frac{(d_{pp}-\lambda_B)^2}{2D} \approx 0.1$ s. Also, in Section 4.1 we estimated from a modified Smoluchowsky equation (Equation (17)) that the typical time scale of the aggregation process, at which most of the particles are found in short chains (dimers) is $t_B \approx 2$ s. As the formation of chains proceeds, (for times larger than $t_B \approx 2$ s) we have new characteristic length and time scales. On the one hand, the diffusion coefficient of chains is substantially smaller than that of single particles and it is anisotropic. For a chain of 10 particles, the parallel and perpendicular diffusion coefficients are 37% and 26% respectively of the diffusion coefficient of a single particle[36], hence the diffusion times for aggregation of chains are also substantially different from those of isolated particles. In addition, the solution becomes more diluted since the typical separation between chains will be larger than the typical separation between initial randomly dispersed particles. As a consequence, in the experiments[35] it was necessary to reach time scales of the order of several minutes to study the aggregation between chains. Therefore, a simulation describing this self-assembly process need to consider all these different time scales discussed so far, from 10^{-4} to 10^2 s, which is of course impossible with a standard simulation technique.

As we said, the appearance of multiple time and length scales is a general aspect of self-assembly problems. This has motivated the development of multiscaling methods[72–75] linking simulations at different resolutions, which are becoming increasingly popular in the Material Sciences. Many of these multi-scaling simulation strategies are specifically adapted to take advantage of special features of each particular problem and thus are designed for solving specific self-assembly problems. Following this tendency, we have proposed a specially designed multi-scaling simulation strategy for the particular problem of magnetic

field induced self-assembly of superparamagnetic colloids in conditions of diffusion dominated kinetics[36], which will be discussed in the following subsection.

4.4 On-the-fly simulation methodology and use of the MagChain® code for quantitative prediction of experimental kinetics

In order to overcome the problems described in the previous subsection, we have introduced a multiscaling strategy[36] (that we called "on-the-fly coarse-graining") for fast and accurate predictions of the formation of chains by superparamagnetic colloids under magnetic fields for the case of kinetics dominated by diffusion ($\Gamma\phi_0 \ll 0.1$) and strong magnetic interactions (large Γ). The algorithm has been implemented in the simulation code MagChain®, which is freely available for scientific use[76].

The basic concept of the methodology can be outlined as follows. In a standard simulation approach, one considers a certain number of simulation objects (atoms, molecules, particles,…) which do not change in nature during the simulation. These simulation objects obey interaction rules and equations of motion that do not change during the simulation. The resolution of a standard simulation (at the electronic scale, atomistic scale, molecular scale, etc) is not changed during the simulation. In our "on-the-fly coarse graining" strategy, the resolution of the simulation is adapted dynamically during the simulation. The objects of the simulation are not fixed a priori at the beginning of the simulation, but rather redefined on the fly. The objects of the simulation can be individual particles or chains of particles. At the beginning of the simulation, the objects of the simulation are only individual particles but as the simulation proceeds, the particles self-assemble in chains. At a given time one has a coexistence of multiple simulation objects (individual particles and chains of different lengths). These chains are treated as individual objects with their own specific interaction rules and equations of motion. In other words, their detailed structure is ignored; the

simulation resolution is at the scale of the chain. The difference with LD simulations is clear (see **Figure 5**). In LD simulations, one takes into account the detailed motion of all the individual particles in a chain, which requires a substantial computational effort (due to the small length scale of the fast vibrational motion of colloids inside a chain). In MagChain, we consider only the collective diffusion of the whole chain, without resolving the individual motion of the particles. Both the dynamics of the simulated objects and their interactions are treated with effective models. The diffusion of the chains is simulated using Brownian dynamics simulations, taking into account an anisotropic diffusion coefficient for the chains (different in parallel and perpendicular directions) which also depends on the length of the chain. The second important simplification made in MagChain is related to the magnetic interactions. Since the exact calculation of the magnetic interactions between simulated objects (particles and chains) is very time consuming, we employ an effective interaction. We consider the magnetic interaction between simulation objects only in the region near each object (particle or chain) in which the attractive magnetic energy of interaction is stronger than the thermal energy. This attraction region is illustrated in Figure 5 for a chain of 5 particles. For simplicity, in the simulations we consider that the attractive region is spherical, which is a good approximation (see Figure 5). We consider that when one object (chain or particle) enters into the attraction region of another object, they aggregate, giving rise to a new, longer chain containing all the particles of the interacting objects. We also neglect the possibility of rupture of chains, an approximation which is valid for large Γ.

This strategy of adapting to the resolution of the self-assembling objects and using a simplified interaction accelerates the simulation by several orders of magnitude. The fact that, as the simulation advances and chains are created, the total number of objects in the system decreases also contributes to accelerate the simulation. This makes possible simulations of processes which are inaccessible by standard techniques. For example, in the particular case presented in section 4.3, using our approach, as implemented in MagChain, we were able to

correctly predict (i.e. in agreement with experimental results) the self-assembly process up to 1000 s (a time scale inaccessible with LD simulations) with a computational cost of only 24 h. It has to be emphasized that the results obtained with the MagChain methodology agree well with results obtained with LD simulations at time scales in which both techniques can be employed[36].

The calculation in MagChain proceeds in two steps[36]. In a first step, one performs a pre-calculation of the radius for the effective magnetic interactions between the objects of the simulation (isolated particles and chains of different lengths). In the second step, one performs the actual simulation. The simulation typically starts with an initial, random distribution of 10^3-10^4 colloids with a given concentration and their motion is simulated in time by using the "on-the-fly" coarse-graining rules previously described.

Let us illustrate the practical use and predictions of this method, with two particular examples. In a MagChain simulation, the input parameters required to predict the kinetics are the average size of the particles (a low polydispersity is assumed), the magnetic characterization of the particles $M=M(H)$, the volume fraction of particles and the viscosity of the dispersing fluid. As an output, it provides the number of chains of different sizes as a function of time. From this information, several quantities can be computed such as the average chain length, the average diffusion coefficient in the directions parallel and perpendicular of the magnetic field or the T_2 response of the system as a function of time.

As a first example, let us consider again the case of sample S5 in Table 1, discussed before in section 4.1 as an example of a very diluted system under strong magnetic fields and with a high magnetic coupling constant (Γ=247 at magnetic saturation). In **Figure 6**, we show the evolution of the average length of the chains as a function of time predicted by MagChain calculations for four different concentrations, from $\phi_0=1.16\times10^{-6}$ to $\phi_0=9.28\times10^{-6}$, corresponding to the NMR experiments performed in Ref[35]. The size of the chains was not directly measured in the experiments, but instead it was measured the T_2 response of the

system as a function of the waiting time under a strong magnetic field. This response can also be computed from an average over MagChain simulation results, since the T_2 response of individual particles or chains is known and the simulation gives the distribution of chains and particles at each time (see Refs[35,36] for details). The results, shown in Figure 6, show a good agreement with experimental results, except for the most concentrated system at very long times in which there were experimental problems related to sedimentation[35]. In this case, the use of MagChain allows one to predict not only the expected change in the response of the system (in this case, T_2) but also allows one to link directly the change in the response of the system with the size distribution of the self-assembled chains, an information which is not accessible experimentally.

As a second example, let us consider the 170 nm colloids shown in Figure 1b. The formation of chains was studied for these colloids at a volume fraction $\phi_0 = 2.6 \times 10^{-5}$ and under a weak external field of 30 mT in Refs[51,68], corresponding to $\Gamma \approx 15$ (employing χ=0.6 in Equation (2) and (8)). Chain formation was studied employing Dynamic Light Scattering (DLS), which provides the time evolution of an average perpendicular diffusion coefficient. Using MagChain simulations, we can obtain the time evolution of the system and compute directly the average value of the diffusion coefficient in the system (in the parallel and perpendicular directions) and the average length of the chains as a function of time. In this case, the applied magnetic field was weak, so we cannot assume that particles are in saturation, as in the previous example. Instead, we employed the full magnetic response M(H) to compute the attractive radius of interaction between particles and chains (see the Supporting Information for full technical details of the simulation). In **Figure 7**, we show the simulation results. The time evolution of the diffusion coefficient obtained from simulations is in excellent agreement with the experimental results. In addition to the diffusion coefficient, which can be compared directly with the experimental results, we also obtain the average size of chains as a function of time which is not directly obtained in the experiments. We see for

example that after half an hour, the average size of the chains is only of 12 particles. The kinetics of self-assembly is therefore very slow in this case.

5. Foundations of the Theory of field-induced self-assembly of Superparamagnetic colloids

In this section, we will discuss the theory that justifies the rules discussed in Section 3. We will also compare our model with other previously proposed models and we will briefly discuss possible extensions.

5.1 Outline of previous theories

From a thermodynamic point of view, superparamagnetic colloids will assemble into chains depending on the balance between two opposite factors, namely the tendency to assembly due to the magnetic interaction energy and the entropic tendency to stay disordered in solution. The objective of a thermodynamic theory is the quantitative prediction of the aggregation state in equilibrium from the knowledge of the magnetic properties of the particles and the thermodynamic conditions (concentration and temperature). The first thermodynamic theory for this problem was formulated by De Gennes and Pincus[6,77] in 1970 and it is still often employed in spite of its limitations. They obtained several results for systems of dipolar particles, and as a particular case they considered a chain of dipoles as shown in **Figure 8**. They considered that under strong fields, colloids will form chains of aligned dipoles, in which the particles are in close contact and the relative orientation θ between the line joining the centers of the particles and the dipoles has thermal fluctuations (see Figure 5). They obtained that in thermodynamic equilibrium these fluctuations decrease as Γ increase ($\langle\theta^2\rangle \sim 1/\Gamma$) and they also obtained an equation for the average length of a chain that in our notation reads:

$$< l >= \left[1 - \frac{8}{3}\phi_0 \frac{e^{\Gamma}}{\Gamma^2}\right]^{-1} . \quad (19)$$

Equation (19) has been widely employed to justify the formation of chains in several experiments[64,78] but it fails to provide even a qualitative prediction. For example, in the case of Ref[78] it predicts negative values for the average length of the chains, which were observed to consist of 4 particles. We have also compiled the predictions of Equation (19) for the simulation data reported in Table 2. The results are summarized in Table 3. As we see, Equation (19) predicts physically unreasonable negative values in several cases. We believe that this unreasonable behavior is due to the truncation of the virial approximation employed in Ref[77] which is of very limited validity. Also, other authors[79] pointed out that the use of the homogeneous fluctuation theory to derive Equation (19) in Ref[77] is incorrect. Therefore, the use of Equation (19) in predictions has to be discouraged.

During the years, there were several alternative thermodynamic theories proposed to study the problem of chain formation by superparamagnetic particles under fields, mainly based in concepts borrowed from polymer theory (see references within Ref[79]). Probably, the first systematic calculation, alternative to the unsatisfactory De Gennes-Pincus approach was that proposed by Zubarev and Iskakova[79], which was based on a direct calculation of the partition function of statistical thermodynamics. The main approximation was to consider only interactions between nearest neighbors, i.e. interactions involving more than two particles were neglected. The authors obtained several analytical results for dipolar particles in magnetic fields. In the case of fully aligned dipoles in a strong external magnetic field, they obtained that the probability of finding a chain containing *l* particles is given by an exponential distribution $p \propto \exp(-\frac{l}{N_Z^*})$ with

$$N_Z^* = \sqrt{\phi_0 \frac{4}{3\Gamma^2} e^{\Gamma}} \quad (20)$$

and the average size of a chain was given by:

$$< l >= \frac{2N_Z^{*2}}{\sqrt{1+4N_Z^{*2}}-2N_Z^{*2}} \approx N_Z^* \quad (21)$$

This result represents an improvement as compared with the De Gennes-Pincus model (Equation (19)) since it always predicts a positive chain length, but it is still unsatisfactory. Equations (20)-(21) systematically predict chain lengths much shorter than obtained in computer simulations, as shown in Table 3.

5.2 **Self-assembly thermodynamics applied to chain formation by superparamagnetic colloids under external magnetic field**

We found[39] that a convenient thermodynamic description for superparamagnetic colloids under magnetic fields can be obtained by adapting to this specific problem well-known thermodynamic theories of self-assembly employed in soft matter[80,81]. We will formulate the problem here with a more general perspective than in our previous works[34,39] in order to show more clearly the relation between our formalism, previous approaches and the thermodynamic theory of self-assembly.

We start by recalling the AMD model, described in Section 2 (see Figure 2). In the presence of an external magnetic field, the colloids develop an asymmetric interaction, with two clearly defined attraction regions in the "front" and in the "back" of the magnetic moment of the particle. We will treat this interaction as a kind of effective directional "magnetic bonding", which is able to create chains of the kind represented in Figure 5 (more complex bundle structures will be discussed later). These directional bonds between particles are broken and created continuously and the thermodynamic equilibrium state will have an equilibrium distribution between structures containing different number of bonds. The equilibrium state will consist of isolated colloids and chains with different lengths, with a distribution to be determined by the "chemical" equilibrium condition: the chemical potential

of an isolated colloid has to be equal to the chemical potential of a colloid in any of the possible self-assembled structures. The chemical potential of an isolated colloid (μ_1) only has an entropic contribution whereas the chemical potential of a colloid inside a chain with *s* colloids (μ_s) contains also an interaction part ($\mu_{int}(s)$) :

$$\mu_1 = \mu_0 + kTln(\phi_1)\,, \tag{22}$$

$$\mu_s = \mu_0 + \frac{1}{s}[kTln(\phi_s/s) + \mu_{int}(s)]\,, \tag{23}$$

where ϕ_1 is the volume fraction of isolated particles in the equilibrium state and ϕ_s is the volume fraction of chains with *s* particles in the equilibrium state, which are related to the initial volume fraction of colloids by $\phi_0 = \sum_{s=1}^{\infty}\phi_s$. If one knows the interaction part of the chemical potential, $\mu_{int}(s)$, then it is possible to determine the composition of the equilibrium state by applying the equilibrium condition $\mu_1 = \mu_2 = \cdots = \mu_s$. The problem is therefore the calculation of $\mu_{int}(s)$, which in principle depends on all possible configurations of the *s* particles of the chain taking into account their relative probabilities and mutual interactions. The approximation of the self-assembly model is to consider that in a chain with *s* colloids there are (*s*–1) "magnetic bonds" between the colloids, so $\mu_{int}(s)$ is given by (*s*–1) times an interaction free energy $-\mu_{bond}$ associated to a single "magnetic bond":

$$\mu_s = \mu_0 + \frac{1}{s}[kTln(\phi_s/s) - (s-1)\mu_{bond}]. \tag{24}$$

With this approximation, it is now possible to obtain significant predictions, in particular to determine the condition for the formation of chains and to obtain explicit expressions for the volume fraction of chains of size *s* and isolated particles (*s*=1) in terms of μ_{bond}. One has to consider Equation (22) and (24), the condition of chemical equilibrium $\mu_1 = \mu_2 = \cdots = \mu_s$, and the definition of ϕ_0. The explicit calculations are analogous to those found in Refs[39,81].

The result is that the nature of the equilibrium state is controlled by a dimensionless parameter N^* given by:

$$N^* = \sqrt{\phi_0 e^{\mu_{bond}/kT}} \tag{25}$$

For $N^* \leq 1$, the equilibrium state consists of isolated particles (no structure) and for $N^* > 1$, the distribution of chains of size s is given approximately by:

$$\frac{\phi_s}{s} \propto \exp(-\frac{s}{N^*}) \tag{26}$$

The average size of a chain can be easily obtained by averaging over the exponential distribution given in Equation (26):

$$< l >= \frac{2N^{*2}}{\sqrt{1+4N^{*2}}-2N^{*2}} \approx N^* \tag{27}$$

Therefore, the thermodynamics of the aggregation behavior is controlled by the values of the volume fraction ϕ_0 and the free energy of the bond between colloids in a chain, μ_{bond}. The problem is now to relate μ_{bond} to the magnetic interaction between particles. We discuss now several possible approximations.

The previous theory of Zubarev and Iskakova[79] discussed in Section 5.1 can be derived by noting that the chemical potential is related to the interaction part of the partition function[81] Z_{int} by $\mu_{bond} \approx \mathrm{kTlnZ_{int}}$. In Ref[79] the authors obtained $\mathrm{Z_{int}} \approx 4e^{\Gamma}/3\Gamma^2$, so we obtain:

$$\mu_{bond} \approx \mathrm{kTln}\left[\frac{4}{3\Gamma^2}e^{\Gamma}\right] \tag{28}$$

Now, we can easily obtain the results discussed in section 5.1 (Equation (20) and (21)) by substituting Equation (28) in Equation (25) and (27). We can see now the reason for the disagreement of this theory with the results of the simulations. In the calculation of the partition function Z_{int}, the authors consider all possible configurations (angles and separations) of two interacting colloidal particles, ignoring the effect of other particles in the system. However, the configurations contributing to μ_{bond} correspond to particles that are forming part of a chain and have a restricted motion due to the interaction with other particles of the

chain. The particles that form a chain can be considered to have a radial motion restricted to be in contact with their neighbors but they have angular fluctuations, as shown schematically in Figure 8. This fact was also recognized by the previous model by de Gennes and Pincus[77].

These considerations also suggest a possible modification of the theory proposed by Zubarev and Iskakova[79]. We have repeated the calculations reported in that work, but considering only angular fluctuations of particles in contact (this is, considering only the configurations corresponding to different values of θ in the calculation of the partition function). With this modification, we obtain for the partition function $Z_{int} \approx 2\pi e^{\Gamma}/3\Gamma$ and

$$\mu_{bond} \approx \mathrm{kTln}\left[\frac{2\pi}{3\Gamma}e^{\Gamma}\right] \quad (29)$$

Again, a modified expression for N^* is obtained by using Equation (29) in Equation (25):

$$N_m^* = \sqrt{\phi_0 \frac{2\pi}{3\Gamma}e^{\Gamma}} \quad (30)$$

As can be seen in Table 3, the predictions of the modified model, using Equation (27) and (30) represent an improvement respect to the predictions of the original Zubarev and Iskakova model.

Finally, let us discuss our mean field approximation[39], which is the basis for the self-assembly rules proposed in Section 3. We note that the free energy of the magnetic bond $-\mu_{bond}$ is approximately equal to the mean magnetic energy of interaction between two particles in contact ($r=d$), assumed to be in a chain as in Figure 8. This is computed by using the magnetic interaction energy given by Equation (3) evaluated for two particles in contact ($r=d$) and averaging over the different orientations θ (θ is defined as in Figure 2 and in Figure 8, i.e. as the angle between the magnetic field and the line joining the centers of the particles). This thermal average of the interaction energy $<U_m(r=d, \theta)>$ is calculated taking into account the probability and energy of the different orientations θ. The result is[39]:

$$-\mu_{bond} \approx < U_m(r=d,\theta) > \cong -kT\left[\frac{U^*}{kT} - 1\right] = -kT[\Gamma - 1], \quad (31)$$

We recover the definition of N^* given in Section 3 (Equation (6)) by substituting Equation (31) in Equation (25). As seen in Table 3, the predictions of this simple approximation are in excellent agreement with the results obtained from computer simulations. This thermodynamic model justifies the classification discussed in Figure 3a and Figure 3b. Now we have to consider its limitations and the appearance of more complex structures.

5.3 Many body magnetic interactions and the formation of bundles of chains in zippered configurations

In the previous section, we have considered the thermodynamics of the formation of chains. However, for systems with strong magnetic interactions (large Γ and consequently large N^*), structures more complex than chains can appear as a consequence of many body magnetic interactions, not considered in the thermodynamic model.

If we consider only the magnetic interactions of a colloid with the nearest neighbor, the configuration corresponding to attractive interactions is that of a tip-to-tip or head-to-tail arrangement, as described in the previous section (see Figure 8) and the only possible structures that can be induced by the magnetic interaction are chains. However, more complex possibilities can arise if we take into account the interaction between all the particles of a chain and an incoming colloid[56]. Let us recall here the energy map shown before in Figure 5 for the magnetic energy of interaction between an incoming colloid and a chain with 5 particles. As discussed earlier, there are two large attractive regions, located at the head and the tail of the chain. Aggregation of a particle in these regions generates a longer chain. But there are also in Figure 5 four small regions at the central region of the chain which correspond to a weak attractive interaction between the incoming particle and the chain. Aggregation of an incoming colloid to one of these locations corresponds to lateral aggregation to the chain, at a midpoint between two particles at the central region of the chain.

It is not difficult to show that these configurations are metaestable. In **Figure 9** we show the energy change due to the addition of an incoming colloid to a chain of N colloids, considering addition in a head-to-tail configuration or in lateral configurations. The calculation has been done by assuming that the chains are made of particles in close contact and adding up numerically all dipole-dipole interactions using Equation (3). As seen in Figure 9a, aggregation of a colloid at the head or the tail of the chain always gives a larger decrease in the magnetic energy of the system. The change in magnetic energy obtained by the lateral addition of a colloid is at best only $-0.18U^*$. The addition of a colloid to a chain gives an energy gain of $\approx -U^*$ for short chains and increases up to a maximum of $\approx -1.2U^*$ for long chains (see Supporting Information for an analytical derivation). Hence, the lateral addition of a particle to a chain corresponds to a metastable state which will tend to relax to a much more favorable state, corresponding to a longer chain. In Figure 9b, we show the energy cost of the restructuring process for relaxation of a laterally aggregated colloid to give a longer chain (again, energy was computed by summing up all dipole-dipole interactions according to Equation (3) for colloids in close contact). The process has an energy barrier, associated to the "opening" of the chain in order to progressively insert the incoming particle. The energy barrier is larger for longer chains than for shorter chains, reaching a saturation value of $0.2U^*$ for long chains. This restructuring process could be possible as a result of thermal fluctuations.

The question is now what happens in the case of interactions between two chains. In the case of a chain with N_1 colloids interacting with a much longer chain with N_2 ($>>N_1$), the results are analogous to those obtained in the previous case. There is always an energetic preference for head-to-tail aggregation, giving a single, longer chain with N_1+N_2 particles, as in the limiting case discussed with $N_1=1$. In the case of lateral aggregation, the resulting two chains in a zipped configuration are in a metastable state and this metastable configuration may also experience restructuring to give a longer aggregate, as described before.

However, the situation changes completely for the case of lateral aggregation of two chains of similar lengths. Lateral aggregation can be energetically favored depending on the length of the interacting chains. For simplicity, let us consider the case of two chains with identical number of particles *N,* as discussed previously in Ref[56]. As shown in **Figure 10**, there is a critical length which corresponds to chains of N_c=14 particles. For $N<N_c$ the minimum energy configuration corresponds to head-to-tail aggregation, leading to a longer chain with 2*N* particles. But for $N>N_c$ lateral aggregation is energetically preferred, so the two chains of *N* particles form a bundle with the two chains in a zipped configuration. This behavior is due to the fact that for lateral aggregation, the decrease in magnetic energy approaches a linear decrease proportional to the number of colloids in the chain, and consequently the energy gain of lateral association always grows with the size of the chains. However, the head-to-tail aggregation of identical chains of *N* colloids gives a decrease in the magnetic energy which depends slightly on the length of the chain, it is $-U^*$ for very short chains and saturates at $\approx -1.64U^*$ for long chains (only the particles in contact and their nearest neighbors really contribute). Therefore, for long enough chains, lateral aggregation has to be preferred.

Let us summarize the results of the magnetic energy calculations reported so far. In the case of the interaction between two chains, there are three possibilities, shown schematically in **Figure 11**. The first possibility is the process of head-to-tail aggregation between two chains, in order to create a longer chain. This process has been observed "in situ" in many experiments, see for example Refs[24,27] and always decreases the magnetic energy, as we have seen here. The second possibility, shown in Figure 11, is the lateral aggregation between chains. This process is possible due to the existence of small regions of attractive magnetic interaction between particles in the central region of the chain, in zipped configurations. In fact, it has been observed experimentally[28] that chains of colloidal particles can attract laterally provided that they are in out of registry, zipped configurations. Our magnetic energy

balance shows that the result of lateral interactions depends strongly on the lengths of the chains, as shown schematically in Figure 11. If one of the chains is much shorter than the other chain, we will observe a restructuring process. The bundle of chains will restructure to give rise to a single, longer chain. This restructuring process can be clearly seen in simulations. We show examples in the movies provided in the Supporting Information, elaborated for this paper using the data of previously reported LD computer simulations[39]. If the two chains are of similar size, and their size is longer than the critical size of 14 particles, the particles will form a thicker aggregate that can be described as a bundle of chains in zipped configuration. Again, these bundles with chains in zippered configurations have been observed[28,30,57] both experimentally and in simulations.

The formation of bundles requires a substantial presence of chains larger than the critical value of 14 particles. Taking into account the exponential distribution given by Equation (26), we can approximately set the onset for the formation of bundles for N^*~10. This is the criterion presented in Section 3 (see also Figure 3c). A prediction of the proportion of particles in bundles and in chains requires an extension of the thermodynamic model described in Section 5.2, which is not available at the present time.

5.4 **Formation of fibrous structures**

At very large values of N^* (which correspond to large values of the magnetic coupling parameter Γ) we can expect that the system contains a large fraction of bundles. The question in this case is whether bundles of two chains in zipped configurations can also grow to give rise to even thicker structures or not. There are several experimental reports of fibrous structures[31,64] which were observed to grow from the lateral interaction between bundles (see for example the videos provided in Ref[31]).

Magnetic calculations analogous to those reported in the previous subsection show that the interaction of a bundle of two chains with a long chain can also lead to the tip to tip

aggregation (making one of the chains longer) or to the lateral aggregation of the third chain, giving rise to a thicker aggregate. This depends again on the length of the interacting chains. In the Supporting Information, we show two examples of the magnetic energy change due to the aggregation of a third chain to a bundle containing two chains. The calculations assume, for simplicity, that the two chains of the bundle have the same length. Repeating systematically these calculations, we have found (**Figure 12**) that lateral aggregation of a third chain to a pre-existing bundle of two chains can be energetically favorable when the pre-existing bundle is made of chains of at least 20 colloids and the third incoming bundle has at least 15 colloids. This thicker aggregate consists of three chains located in the same plane, i.e. non coplanar aggregation it is never preferred energetically.

6. **Conclusion**

In this work, we have revisited recent advances in the quantitative prediction of self-assembly of superparamagnetic colloids under a magnetic field. The external field induces in each colloid a magnetic dipole in the field direction; as a consequence, colloids interact magnetically and can generate self-assembled anisotropic structures. In some applications of superparamagnetic colloids, self-assembly is desired (magnetophoresis,…) while in others it is clearly an unwanted effect (IMR, drug delivery,…). Thus, in the design of magnetic particles and experimental protocols it is desirable to predict under what circumstances (particle features and thermodynamic conditions) self-assembly will occur.

Our focus here has been on theoretical methodologies that can be used in practice to predict the equilibrium self-assembled states and the dynamics of self-assembly in terms of basic particle characterization data (size and magnetic response) and experimental conditions (concentration and temperature). A key result is that the self-assembled equilibrium state can be fully characterized by a single dimensionless parameter, the aggregation parameter N^*,

which depends on the properties of the colloids (diameter and magnetic response) but also on thermodynamic variables: the concentration of colloids and the temperature. Self-assembly of superparamagnetic colloids will not occur for $N^* < 1$ (too diluted systems or too weak magnetic interactions). For $N^* > 1$, colloids will self-assembly in anisotropic structures, such as chains with an average length of approximately N^* particles ($1<N^*<10$), chains and bundles of zipped chains ($N^* > 10$) and bundles of zipped chains and fibrous structures ($N^* >> 10$).

We have also discussed the kinetic aspects of self-assembly. Under typical experimental conditions, the kinetics can be dominated by magnetic interactions (fast kinetics) or by diffusion (slow kinetics). We have provided a quantitative rule to determine the conditions under which mechanism dominates depending on the strength of magnetic interactions and the concentration of the suspension. The most challenging situation corresponds to the case of very slow kinetics observed in the case of very low volume fraction of colloids and strong magnetic interactions. In this case, the equilibrium state (which typically correspond to large values of N^*) is not accessible under experimental time scales, and only kinetic predictions are relevant. Under these circumstances, quantitative prediction of the kinetics of self-assembly from the properties of the particles and the suspension (particle size, magnetization, concentration, temperature, solvent viscosity) requires the use of specially designed multi-scaling simulation techniques. Standard simulation techniques cannot be employed in this case, due to the coexistence of multiple time and length scales. As we have shown in two particular examples, our novel coarse-grained methodology implemented in the simulation code MagChain®, successfully predicts the results of NMR or DLS experiments from time scales of miliseconds to several minutes.

Of course, there are still many open problems which deserve further attention from theorists. The models described so far consider only static fields. In certain applications, the direction of the magnetic field rotates[18] and depending on the frequency of the rotating field, self-assembled structures may be able or not to follow the magnetic field and new phenomena

may appear. Also, it is relevant to include other typical colloidal interactions in the models, such as electrostatic interactions since there are interesting experimental examples in which self-assembled structures are influenced by the addition of salt[25,82]. We expect to be able to provide further predictive tools in the future, which will help to advance in the long term goal of providing useful tools for the rational design of materials and self-assembly processes.

Supporting Information ((delete if not applicable))
Supporting Information is available from the Wiley Online Library or from the author.

Acknowledgements

((Acknowledgements, general annotations, funding. Other references to the title/authors can also appear here, such as "Author 1 and Author 2 contributed equally to this work."))

Received: ((will be filled in by the editorial staff))
Revised: ((will be filled in by the editorial staff))
Published online: ((will be filled in by the editorial staff))

[1] C. Kittel, *Phys. Rev.* **1946**, *70*, 965.

[2] C. Kittel, *Rev. Mod. Phys.* **1949**, *21*, 541.

[3] C. P. Bean, J. D. Livingston, *J. Appl. Phys.* **1959**, *30*, S120.

[4] S. Singamaneni, V. N. Bliznyuk, C. Binek, E. Y. Tsymbal, *J. Mater. Chem.* **2011**, *21*, 16819.

[5] A.-H. Lu, E. L. Salabas, F. Schüth, *Angew. Chem. Int. Ed. Engl.* **2007**, *46*, 1222.

[6] R. E. Rosensweig, *Ferrohydrodynamics*; 1st ed.; Cambridge university Press: Cambridge [etc.] :, 1985.

[7] I. Torres-Díaz, C. Rinaldi, *Soft Matter* **2014**, *10*, 8584.

[8] A. Tokarev, Y. Gu, A. Zakharchenko, O. Trotsenko, I. Luzinov, K. G. Kornev, S. Minko, *Adv. Funct. Mater.* **2014**, *24*, 4738.

[9] X. Xu, G. Friedman, K. D. Humfeld, S. A. Majetich, S. A. Asher, *Chem. Mater.* **2002**, *14*, 1249.

[10] J. Ge, Y. Hu, Y. Yin, *Angew. Chemie Int. Ed.* **2007**, *46*, 7334.

[11] J. L. Corchero, A. Villaverde, *Trends Biotechnol.* **2009**, *27*, 468.

[12] B. Kozissnik, A. C. Bohorquez, J. Dobson, C. Rinaldi, *Int. J. Hyperth.* **2013**.

[13] Q. A. Pankhurst, N. T. K. Thanh, S. K. Jones, J. Dobson, *J. Phys. D. Appl. Phys.* **2009**, *42*, 224001.

[14] M. Colombo, S. Carregal-Romero, M. F. Casula, L. Gutiérrez, M. P. Morales, I. B. Böhm, J. T. Heverhagen, D. Prosperi, W. J. Parak, *Chem. Soc. Rev.* **2012**, *41*, 4306.

[15] C. T. Yavuz, A. Prakash, J. T. Mayo, V. L. Colvin, *Chem. Eng. Sci.* **2009**, *64*, 2510.

[16] G. Friedman, B. Yellen, *Curr. Opin. Colloid Interface Sci.* **2005**, *10*, 158.

[17] J. Lim, S. P. Yeap, S. C. Low, *Sep. Purif. Technol.* **2014**, *123*, 171.

[18] M. Berenguel-Alonso, X. Granados, J. Faraudo, J. Alonso-Chamarro, M. Puyol, *Anal. Bioanal. Chem.* **2014**, *406*, 6607.

[19] G. Fonnum, C. Johansson, A. Molteberg, S. Mørup, E. Aksnes, *J. Magn. Magn. Mater.* **2005**, *293*, 41.

[20] E. Taboada, R. Solanas, E. Rodríguez, R. Weissleder, A. Roig, *Adv. Funct. Mater.* **2009**, *19*, 2319.

[21] D. Hritcu, D. Humelnicu, G. Dodi, M. I. Popa, *Carbohydr. Polym.* **2012**, *87*, 1185.

[22] V. Salgueiriño-Maceira, M. A. Correa-Duarte, M. Spasova, L. M. Liz-Marzán, M. Farle, *Adv. Funct. Mater.* **2006**, *16*, 509.

[23] O. Tagit, N. Tomczak, E. M. Benetti, Y. Cesa, C. Blum, V. Subramaniam, J. L. Herek, G. Julius Vancso, *Nanotechnology* **2009**, *20*, 185501.

[24] J. H. E. Promislow, A. P. Gast, M. Fermigier, *J. Chem. Phys.* **1995**, *102*, 5492.

[25] F. Martínez-Pedrero, A. El-Harrak, J. C. Fernández-Toledano, M. Tirado-Miranda, J. Baudry, A. Schmitt, J. Bibette, J. Callejas-Fernández, *Phys. Rev. E* **2008**, *78*, 011403.

[26] S. Relle, S. B. Grant, C. Tsouris, *Phys. A Stat. Mech. its Appl.* **1999**, *270*, 427.

[27] G. P. Gajula, M. T. Neves-Petersen, S. B. Petersen, *Appl. Phys. Lett.* **2010**, *97*, 103103.

[28] E. M. Furst, A. P. Gast, *Phys. Rev. E* **2000**, *62*, 6916.

[29] J. M. Laskar, J. Philip, B. Raj, *Phys. Rev. E* **2009**, *80*, 041401.

[30] D. Heinrich, A. R. Goñi, A. Smessaert, S. H. L. Klapp, L. M. C. Cerioni, T. M. Osán, D. J. Pusiol, C. Thomsen, *Phys. Rev. Lett.* **2011**, *106*, 208301.

[31] G. DeLasCuevas, J. Faraudo, J. Camacho, *J. Phys. Chem. C* **2008**, *112*, 945.

[32] O. Trotsenko, A. Tokarev, A. Gruzd, T. Enright, S. Minko, *Nanoscale* **2015**, *7*, 7155.

[33] J. Andreu, J. Camacho, J. Faraudo, M. Benelmekki, C. Rebollo, L. Martínez, *Phys. Rev. E* **2011**, *84*, 1.

[34] J. Faraudo, J. S. Andreu, J. Camacho, *Soft Matter* **2013**, *9*, 6654.

[35] D.-X. Chen, G. Via, F.-J. Xu, C. Navau, A. Sanchez, H.-C. Gu, J. S. Andreu, C. Calero, J. Camacho, J. Faraudo, *J. Appl. Phys.* **2011**, *110*, 073917.

[36] J. S. Andreu, C. Calero, J. Camacho, J. Faraudo, *Phys. Rev. E* **2012**, *85*, 036709.

[37] S. L. Saville, R. C. Woodward, M. J. House, A. Tokarev, J. Hammers, B. Qi, J. Shaw, M. Saunders, R. R. Varsani, T. G. St Pierre, O. T. Mefford, *Nanoscale* **2013**, *5*, 2152.

[38] S. L. Saville, B. Qi, J. Baker, R. Stone, R. E. Camley, K. L. Livesey, L. Ye, T. M. Crawford, O. T. Mefford, *J. Colloid Interface Sci.* **2014**, *424*, 141.

[39] J. S. Andreu, J. Camacho, J. Faraudo, *Soft Matter* **2011**, *7*, 2336.

[40] M. Antonietti, S. Förster, *Adv. Mater.* **2003**, *15*, 1323.

[41] K. M. Krishnan, A. B. Pakhomov, Y. Bao, P. Blomqvist, Y. Chun, M. Gonzales, K. Griffin, X. Ji, B. K. Roberts, *J. Mater. Sci.* **2006**, *41*, 793.

[42] W. T. Coffey, Y. P. Kalmykov, *J. Appl. Phys.* **2012**, *112*, 121301.

[43] I. Torres-Díaz, C. Rinaldi, *Soft Matter* **2014**, *10*, 8584.

[44] K. Butter, P. H. H. Bomans, P. M. Frederik, G. J. Vroege, A. P. Philipse, *Nat. Mater.* **2003**, *2*, 88.

[45] M. Klokkenburg, C. Vonk, E. M. Claesson, J. D. Meeldijk, B. H. Erné, A. P. Philipse, *J. Am. Chem. Soc.* **2004**, *126*, 16706.

[46] V. F. Puntes, P. Gorostiza, D. M. Aruguete, N. G. Bastus, A. P. Alivisatos, *Nat. Mater.* **2004**, *3*, 263.

[47] M. Klokkenburg, R. P. A. Dullens, W. K. Kegel, B. H. Erné, A. P. Philipse, *Phys. Rev. Lett.* **2006**, *96*, 037203.

[48] M. Varón, L. Peña, L. Balcells, V. Skumryev, B. Martinez, V. Puntes, *Langmuir* **2010**,

26, 109.

[49] D.-X. Chen, A. Sanchez, E. Taboada, A. Roig, N. Sun, H.-C. Gu, *J. Appl. Phys.* **2009**, *105*, 083924.

[50] V. Singh, V. Banerjee, *J. Appl. Phys.* **2012**, *112*, 114912.

[51] F. Martínez-Pedrero, M. Tirado-Miranda, A. Schmitt, J. Callejas-Fernández, *J. Colloid Interface Sci.* **2008**, *318*, 23.

[52] S. Yu, J. A. Hachtel, M. F. Chisholm, S. T. Pantelides, A. Laromaine, A. Roig, *Nanoscale* **2015**, *7*, 14039.

[53] K. J. M. Bishop, C. E. Wilmer, S. Soh, B. A. Grzybowski, *Small* **2009**, *5*, 1600.

[54] H. Zhang, M. Widom, *Phys. Rev. E* **1995**, *51*, 2099.

[55] S. S. Leong, Z. Ahmad, J. Lim, *Soft Matter* **2015**, *11*, 6968.

[56] J. Faraudo, J. Camacho, *Colloid Polym. Sci.* **2009**, *288*, 207.

[57] D. Heinrich, A. R. Goñi, T. M. Osán, L. M. C. Cerioni, A. Smessaert, S. H. L. Klapp, J. Faraudo, D. J. Pusiol, C. Thomsen, *Soft Matter* **2015**.

[58] C. Cheng, F. Xu, H. Gu, *New J. Chem.* **2011**, *35*, 1072.

[59] M. Popovici, M. Gich, D. Nižňanský, A. Roig, C. Savii, L. Casas, E. Molins, K. Zaveta, C. Enache, J. Sort, S. de Brion, G. Chouteau, J. Nogués, *Chem. Mater.* **2004**, *16*, 5542.

[60] S. P. Yeap, S. S. Leong, A. L. Ahmad, B. S. Ooi, J. Lim, *J. Phys. Chem. C* **2014**, *118*, 24042.

[61] P. Hertz, *Math. Ann.* **1909**, *67*, 387.

[62] S. Chandrasekhar, *Rev. Mod. Phys.* **1943**, *15*, 1.

[63] M. Abramowitz, I. A. Stegun, *Handbook of mathematical functions : with formulas, graphs, and mathematical tables*; Dover: New York :, 1972.

[64] M. Fermigier, A. P. Gast, *J. Colloid Interface Sci.* **1992**, *154*, 522.

[65] P. Domínguez-García, S. Melle, J. M. Pastor, M. A. Rubio, *Phys. Rev. E* **2007**, *76*, 051403.

[66] P. Domínguez-García, S. Melle, M. A. Rubio, *J. Colloid Interface Sci.* **2009**, *333*, 221.

[67] M. Hagenbüchle, J. Liu, *Appl. Opt.* **1997**, *36*, 7664.

[68] F. Martínez-Pedrero, M. Tirado-Miranda, A. Schmitt, J. Callejas-Fernández, *Phys. Rev. E* **2007**, *76*, 011405.

[69] V. Singh, V. Banerjee, M. Sharma, *J. Phys. D-Applied Phys.* **2009**, *42*, 245006.

[70] S. Plimpton, *J. Comput. Phys.* **1995**, *117*, 1.

[71] C.-A. Palma, M. Cecchini, P. Samorì, *Chem. Soc. Rev.* **2012**, *41*, 3713.

[72] L. Visscher, P. Bolhuis, F. M. Bickelhaupt, *Phys. Chem. Chem. Phys.* **2011**, *13*, 10399.

[73] A. Mirzoev, A. P. Lyubartsev, *J. Chem. Theory Comput.* **2013**, *9*, 1512.

[74] C. Peter, K. Kremer, *Soft Matter* **2009**, *5*, 4357.

[75] T. J. Roussel, E. Barrena, C. Ocal, J. Faraudo, *Nanoscale* **2014**, *6*, 7991.

[76] J. Andreu, Jordi; Calero, Carles; Camacho, Juan; Faraudo, MagChain simulation website. *http://departments.icmab.es/softmattertheory/*.

[77] P. G. Gennes, P. A. Pincus, *Phys. der Kondens. Mater.* **1970**, *11*, 189.

[78] M. Barrett, A. Deschner, J. P. Embs, M. C. Rheinstädter, *Soft Matter* **2011**, *7*, 6678.

[79] A. Y. Zubarev, L. Y. Iskakova, *Phys. Rev. E* **2002**, *65*, 061406.

[80] J. N. Israelachvili, *Intermolecular and surface forces*; Academic Press: London [etc.] :, 1992.

[81] S. A. Safran, *Statistical thermodynamics of surfaces, interfaces and membranes*;

Addison-Wesley, 1994.

[82] S. P. Yeap, A. L. Ahmad, B. S. Ooi, J. Lim, *Langmuir* **2012**, *28*, 14878.

[83] F. Martinez Pedrero, PhD Thesis: Colloidal aggregation induced by an uniaxial magnetic field, Universidad de Granada, 2008.

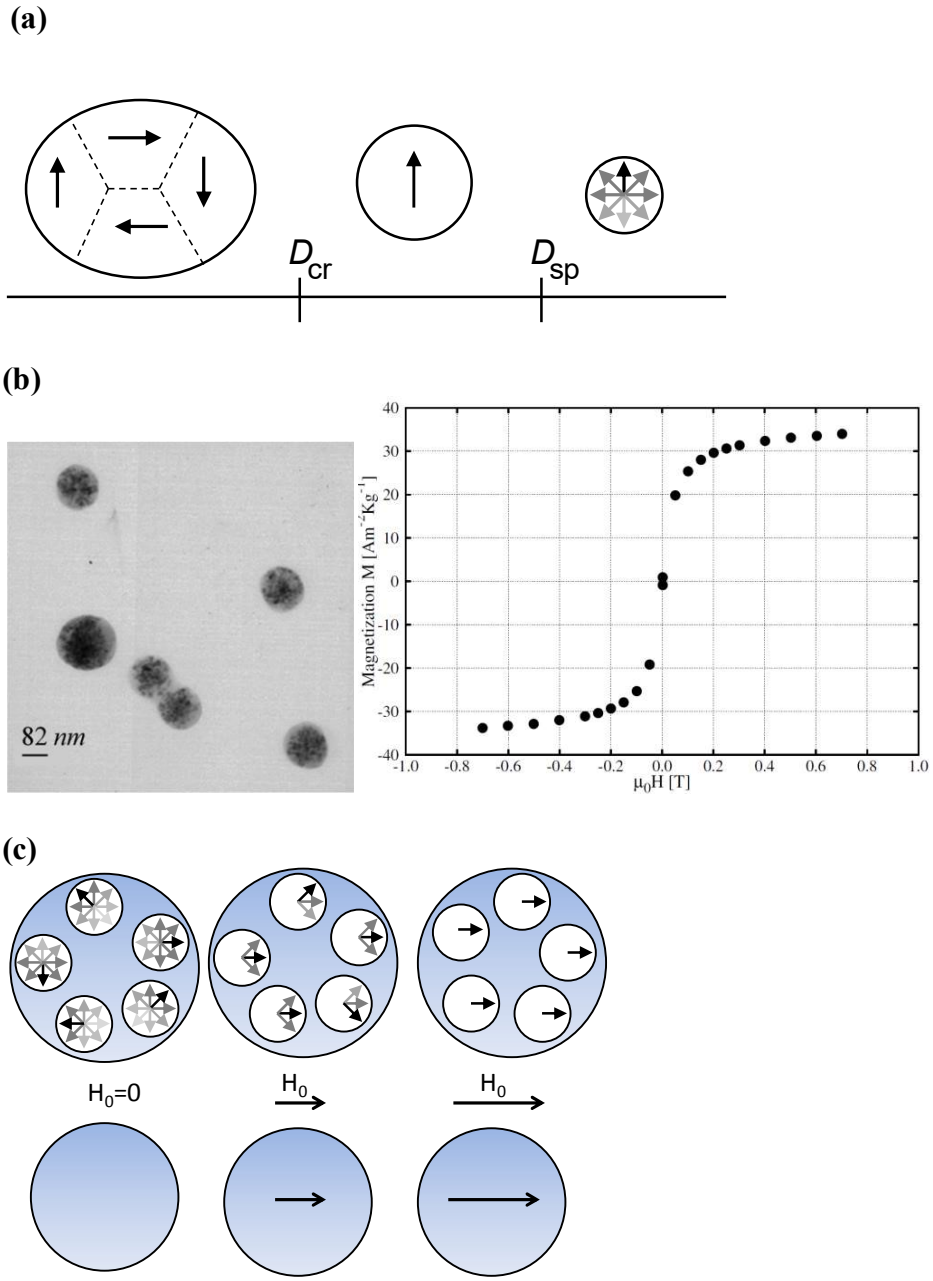

Figure 1. (a) Cartoon indicating the different behavior of magnetic particles depending on its size (multidomain, single domain or superparamagnetic) (b) Images and magnetic response of polystyrene colloids containing superparamagnetic NP inside (dark spots) employed in the self-assembly experiments in Refs[51]. (c) Illustration of the nanoscopic origin of the magnetic behavior of the superparamagnetic colloid in absence and in presence of a magnetic field. The colloid contains many NPs, and each of these NPs has an unstable magnetic moment that freely rotates in all directions (Neel relaxation) when H=0. For H≠0, the moments of the nanoparticles fluctuate around the direction of the external field. Under sufficiently strong H fields the magnetic moments of the nanoparticles become completely aligned to the applied external field. In all these cases, the magnetic response of the colloid can be represented with a magnetic dipole aligned to the external field, with an intensity that increases with the intensity of the applied field and is zero in absence of external field.
Left image in (b) reproduced with permission from Ref[83]

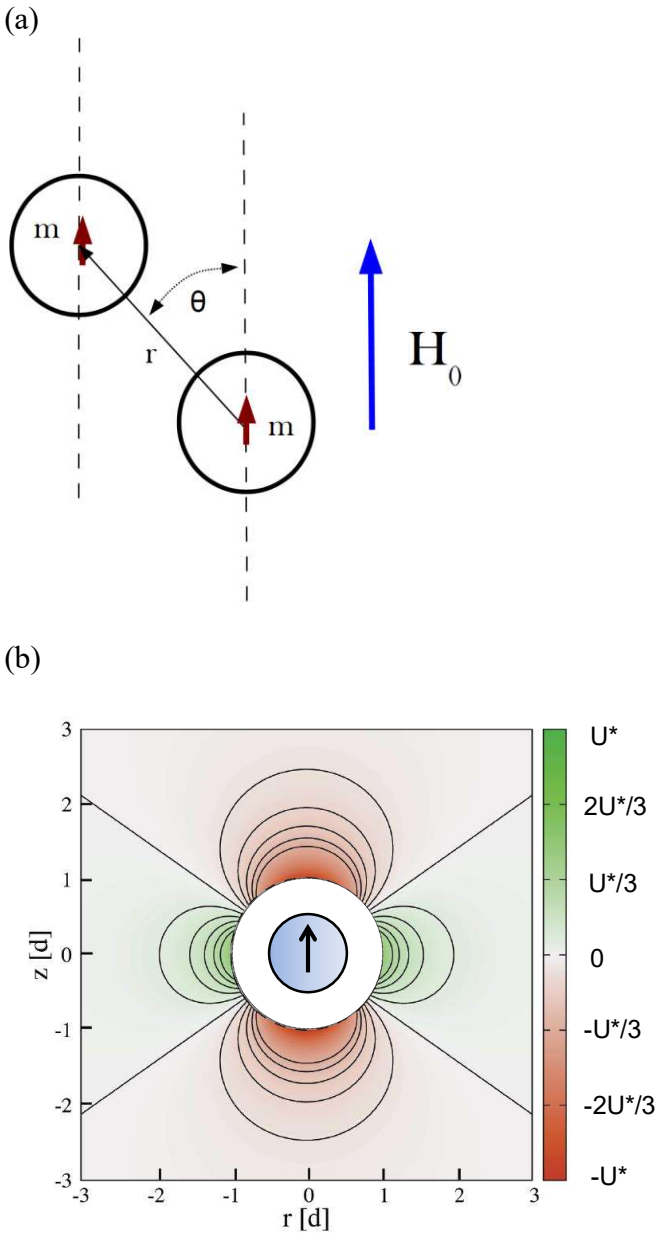

Figure 2. (a) Scheme indicating the geometry of the interaction between two colloidal particles with dipolar moment *m* in the direction of an external magnetic field. (b) Magnetic dipole–dipole interaction energy (Equation (3) and (4)) between the particle shown in the center of the figure and an imaginary test particle. The black arrow indicates the dipole of the particle, pointing in the direction of the apllied magnetic field (*z* axis). The distance (in cylindrical coordinates) is measured in units of the diameters of the particle *d*. The red color corresponds to attractive regions (negative energy) and the green color corresponds to repulsive regions (positive energy).

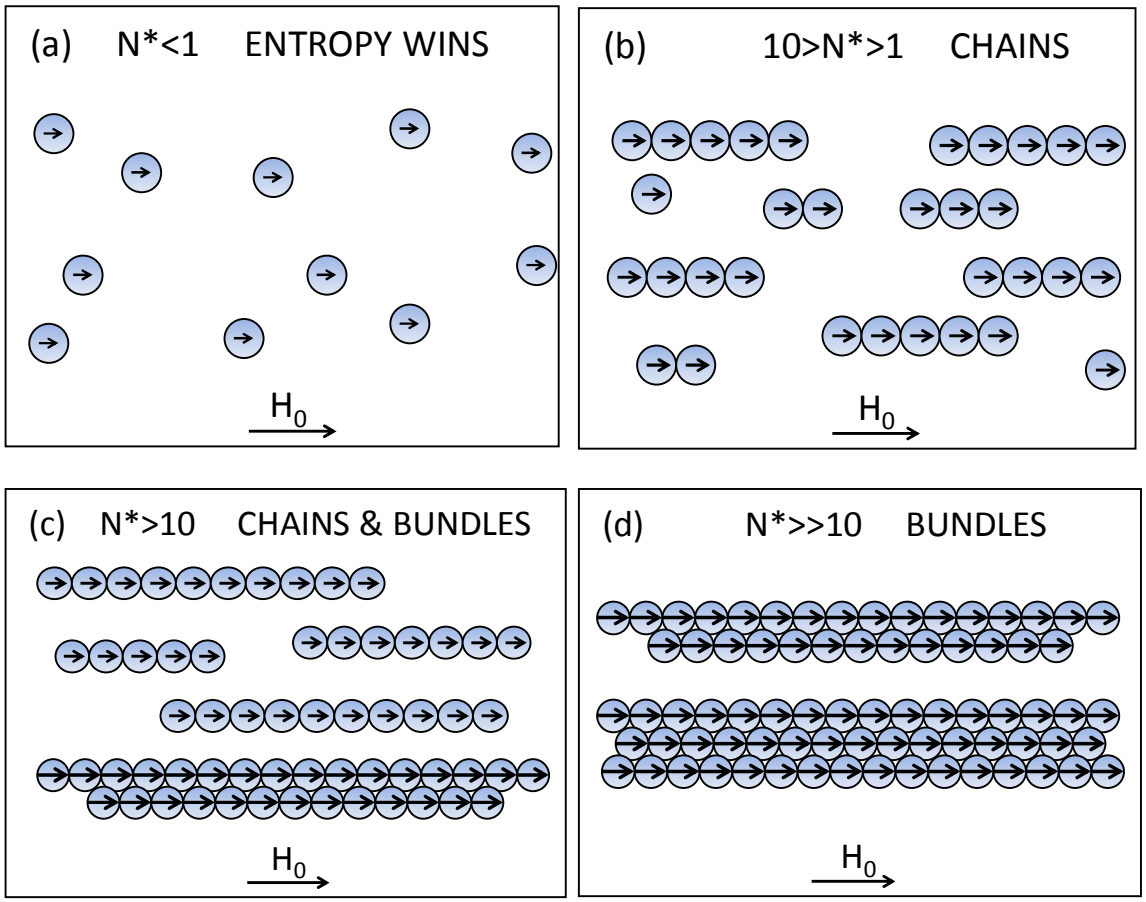

Figure 3. Scheme summarizing the self-assembly behavior of superparamagentic colloids under an external magnetic field according to the value of the aggregation parameter N^* defined in Equation (6). (a) no self-assembly; (b) equilibrium state consisting of chains of different sizes with an average length given by Equation (9); (c) Equilibrium state consisting of long chains and bundles of laterally aggregated chains in zipped, out-of registry, configuration; (d) Equilibrium state consisting of bundles of laterally aggregated chains.

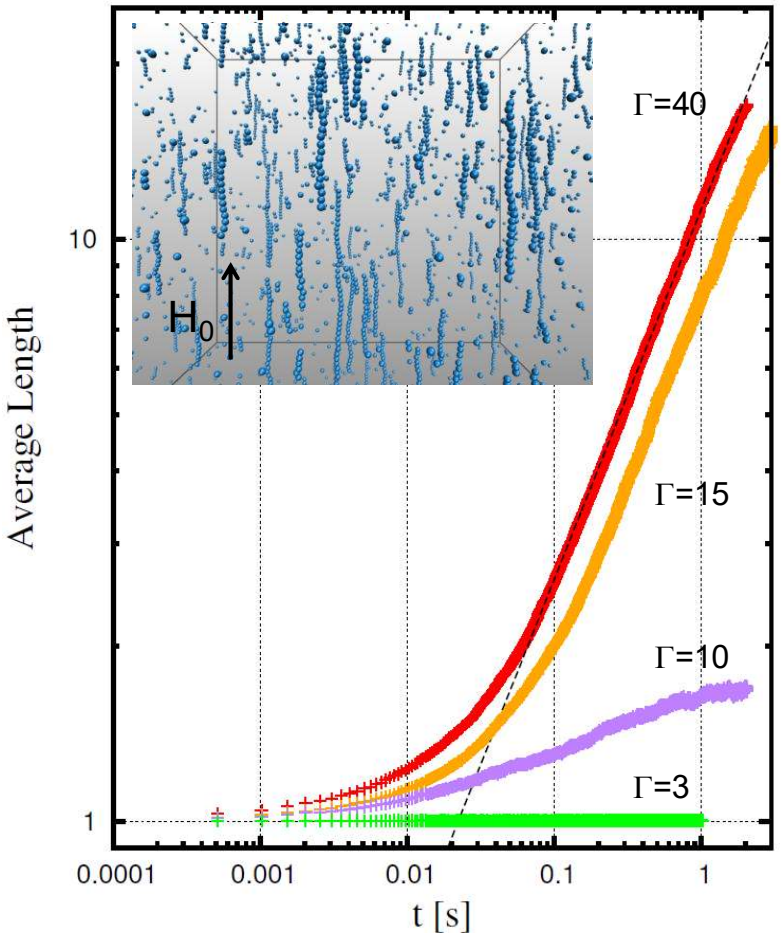

Figure 4. Time evolution of the average length of chains of superparamagnetic colloids under strong magnetic field as obtained from LD computer simulations (data from[39]). All simulations correspond to a volume fraction of $\phi_0=5.23\times10^{-4}$ and different values of Γ. The dashed line shows a fit of the data for Γ=40 to a power law t^z with exponent z=0.64. Inset: simulation snapshot for Γ=40.

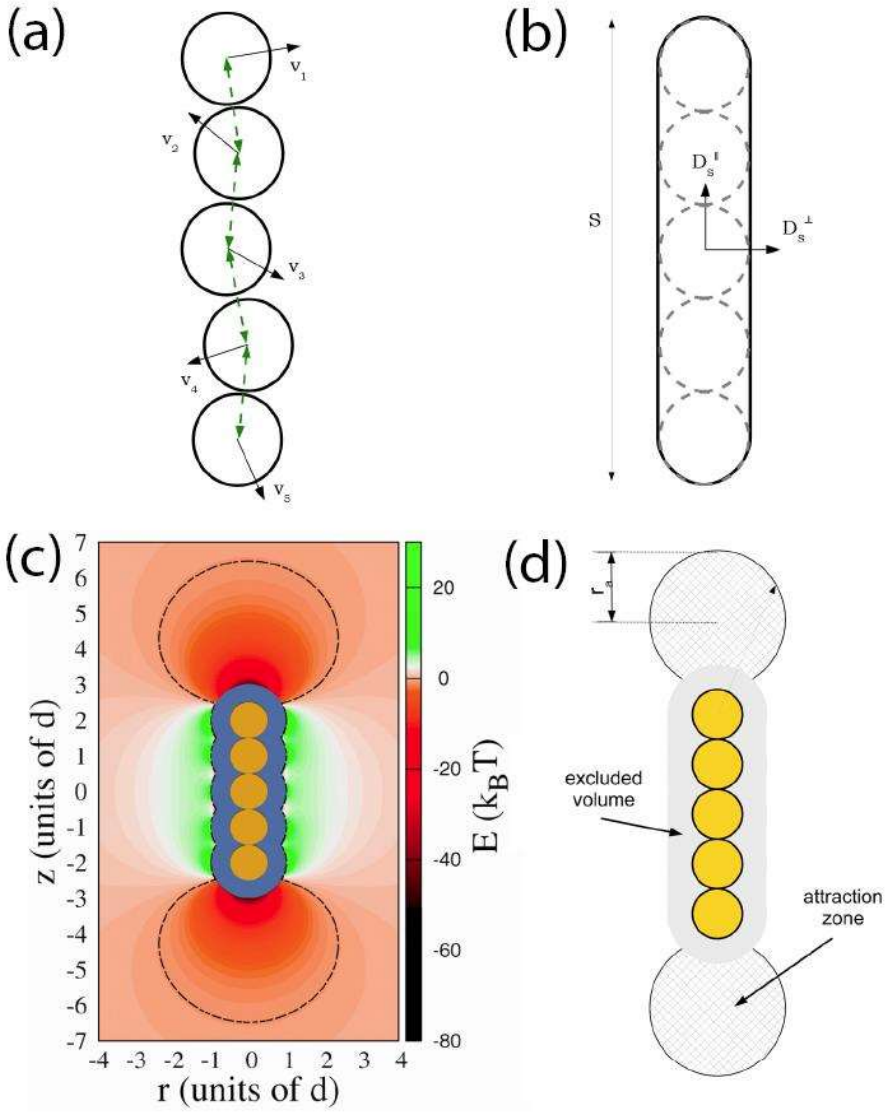

Figure 5. (a) Motion of colloids in a chain in a LD simulation; (b) Effective ellipsoid representing a chain of *s* colloids, which has anisotropic diffusion with different coefficients in the parallel and perpendicular directions. (c) Map of magnetic potential energy of interaction between an imaginary colloid and a chain of 5 particles, all magnetized in the *z* direction. The calculation corresponds to Γ=40 and the magnetic energy is measured in units of $k_B T$. The dashed line indicates the regions at which the magnetic energy is equal (in absolute value) to the thermal energy. (d) Coarse grain representation of the chain in (c) as employed in MagChain simulations, in which the attractive region inside the dashed lines in (c) is replaced by a spherical region.

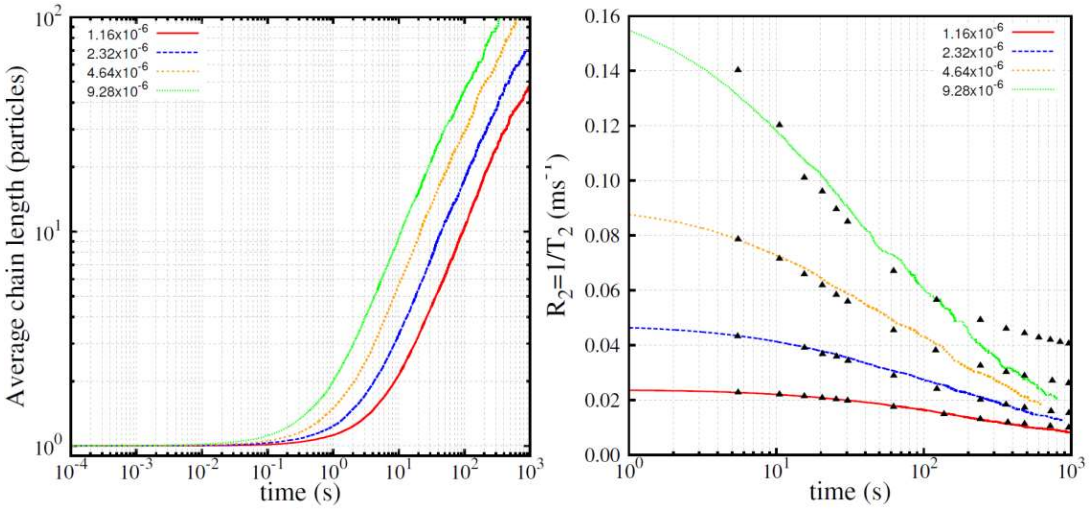

Figure 6. Kinetics of chain formation for 88 nm superparamagnetic colloids under a strong magnetic field (Γ=247) and different volume fractions: 1.16×10^{-6} , 2.32×10^{-6} , 4.64×10^{-6} and 9.28×10^{-6} (data from Ref[36]). Left: average length of chains as a function of time calculated from MagChain simulations. Right: time evolution of the transversal relaxation time as measured in NMR under the same conditions as in the left figure. The dots correspond to experimental data and the lines to the prediction calculated from MagChain simulations. Comparing the left and right figures one can directly relate the relaxation rate observed at a given time to the corresponding aggregation state at that time.

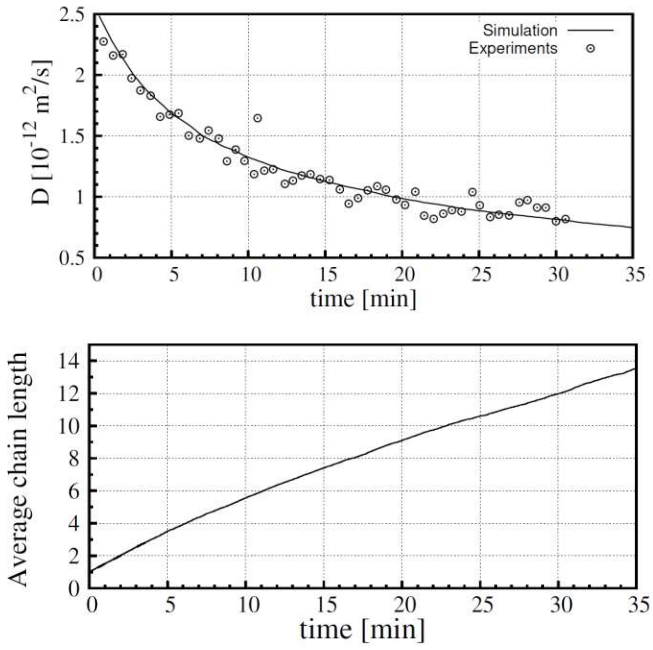

Figure 7. Kinetics of chain formation under a 30 mT magnetic field for a colloidal suspension with a volume fraction of 2.6×10^{-5} of the particles shown in Figure 1b. Top: Effective diffusion coefficient obtained from DLS measurements[68] (dots) and predicted from MagChain simulations (solid line). Bottom: average length of chains as a function of time calculated from MagChain simulations. Comparing the top and bottom figures one can directly relate the change observed in the diffusion coefficient at a given time to the corresponding self-assembly state at that time.

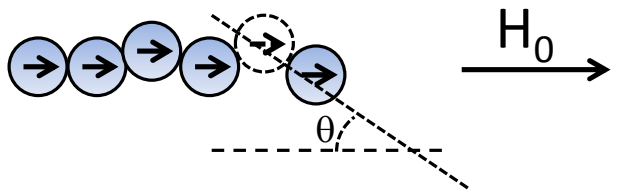

Figure 8. Scheme of a chain of superparamagnetic colloids induced by a magnetic field with fluctuations in the positions of the particles of the chain.

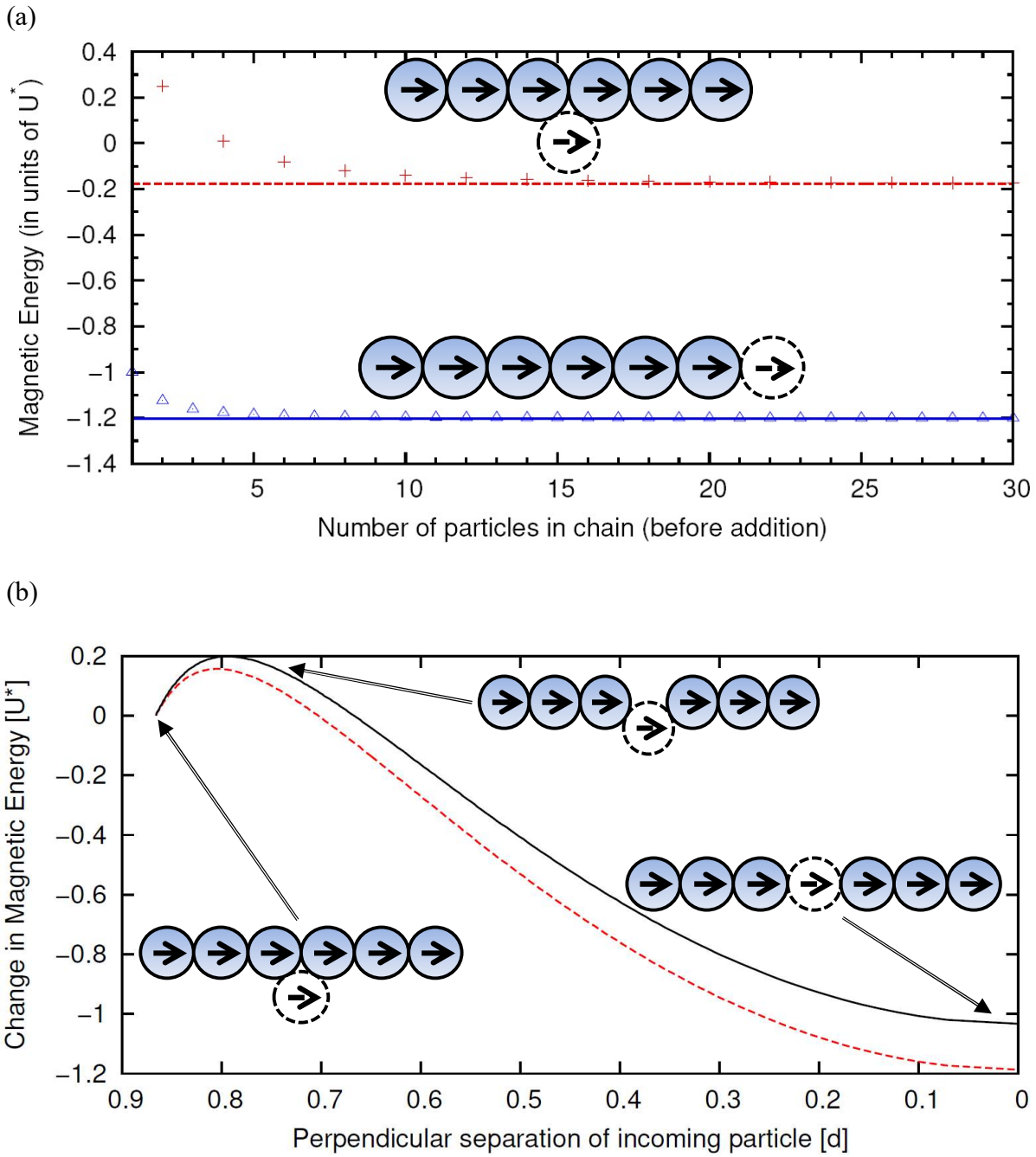

Figure 9. Results from magnetic energy calculations. (a) Change in magnetic energy due to the addition of one colloid to a chain of colloids at different positions: at the head or at the tail of the chain or at a lateral position. (b) Change in magnetic energy in a restructuring process. In this process, an incoming colloid is initially aggregated laterally to a chain. The chain gradually opens (a process with an energy barrier) to allow the colloid to penetrate into the chain, and finally the colloid is incorporated into the chain with a concomitant decrease in the magnetic energy of the system. The dashed line corresponds to a chain with 4 colloids and the solid line to a chain with 20 colloids (which is close to the asymptotic value for very large chains). The magnetic energy scale U^* is defined in Equation (4).

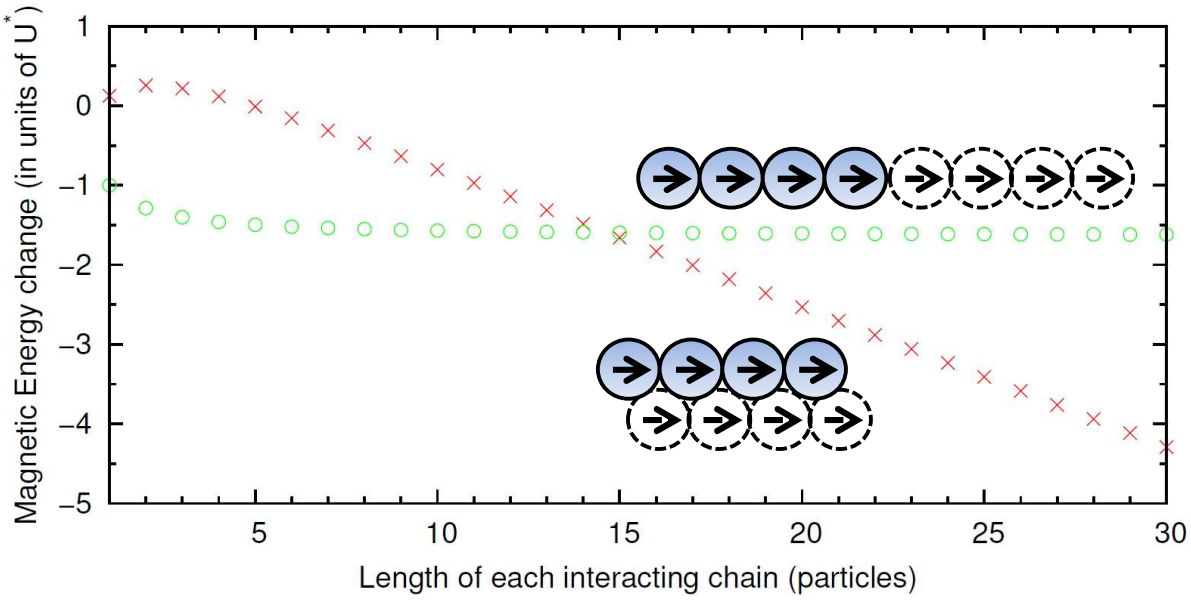

Figure 10. Change in magnetic energy due to the aggregation of two chains with identical number of particles. We compare two possibilities: head-to-tail aggregation, which gives as a result a longer chain (circles) or lateral aggregation in a zippering configuration, which produces a thicker chain (crosses). The magnetic energy scale U^* is defined in Equation (4).

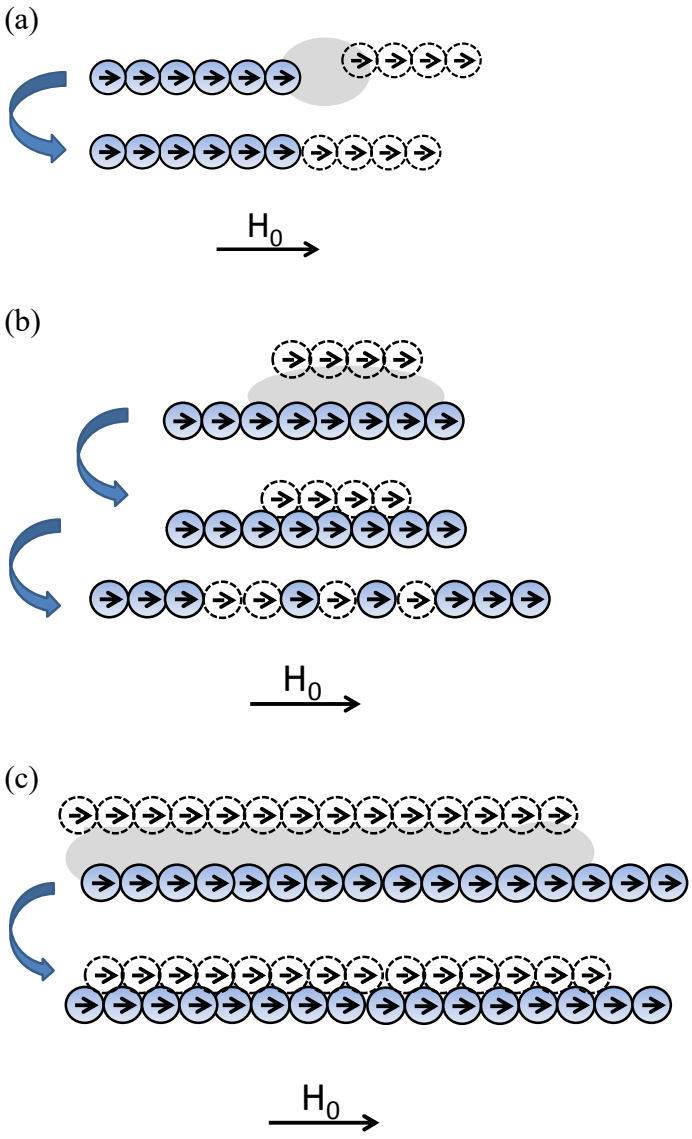

Figure 11. Summary of possible results for the interaction between two chains of colloids as deduced form the calculations in Figure 9 and 10. (a) head-to-tail aggregation, which always reduces the magnetic energy between tails. (b) Lateral aggregation between chains with less than 14 colloids. In this case, a restructuration process generates a single chain. (c) Lateral aggregation of long chains. In this case, a bundle with two chains in zippering configuration is formed.

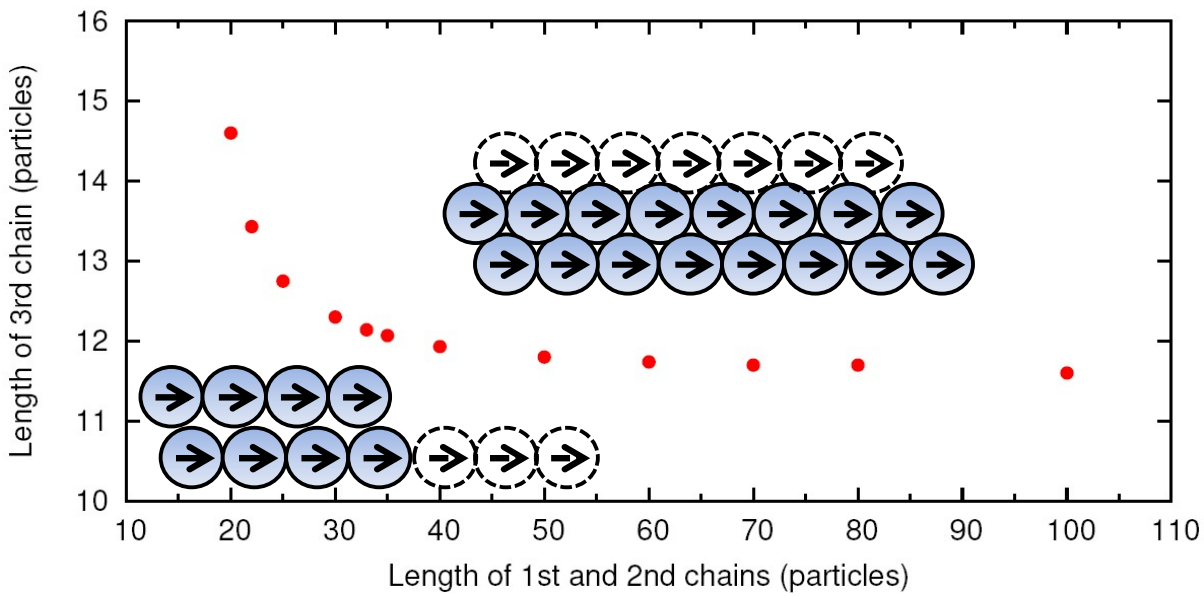

Figure 12. Diagram indicating the configuration of minimum magnetic energy corresponding to the addition of a third chain of arbitrary length to a pre-existing bundle of two identical chains. The dots show the frontier between the two possible final configurations: a bundle with three chains in zippering configuration (lateral aggregation) or a bundle with two chains (head-to-tail aggregation).

Table 1. Summary of physical properties and calculated Γ, ϕ_0 and N^* parameters (Equation (7), (8) and (9)) for several composite superparamagnetic colloids under strong magnetic fields.

S#, Material and Reference	diameter [nm]	M_s [Am^2Kg^{-1}]	ρ [Kgm^{-3}]	Γ a)	c [$g\ L^{-1}$]	ϕ_0	N^*
S1 Core (γ-Fe_2O_3)/Shell (SiO_2)[20]	82	4.4	2270	0.7	1.0	4.4×10^{-4}	0.02
S2 Core (γ-Fe_2O_3)/Shell (SiO_2)[20]	157	3.7	2290	3.7	1.0	4.4×10^{-4}	0.08
S3 Fe_3O_4 clusters -PEG[55]	31	42.7	3455	7.8	0.1	2.9×10^{-5}	0.16
S4 Fe_3O_4 clusters-surfactant[30,57]	145	NA b)	NA	12	NA	10^{-2}	24
S5 Fe_3O_4 clusters-EG/PG[35,58]	88	63.8	3100	247	0.014	$1.2\text{-}9.3\times10^{-6}$	$\sim10^{50}$-10^{51}
S6 Fe_3O_4 clusters- polymer[37]	106	70.0	3328	395	3.3	10^{-3}	$\sim10^{84}$

a) Assuming T=298K except in S4 (T=310 K); **b**) The dipolar moment of the particles was reported in Ref[30,57] instead of saturation magnetization (m=2.744×10^{-17} J/T). Density was not available.

Table 2. Summary of results from computer simulations in Ref[39] (simulations S1 to S6) and Ref[57] (simulation S7) for colloids at magnetic saturation due to an external magnetic field. We indicate the observed structures at saturation magnetization and the average length of the structures obtained in simulations in the direction of the applied field $< l >_{\mathrm{sim}}$ (measured in number of particles). Each simulation corresponds to a different combination of volume fraction ϕ_0 and magnetic coupling parameter Γ. The reported aggregation parameter N^* is calculated using Equation (6).

Simulation number	Structures	$< l >_{\mathrm{sim}}$	Γ	ϕ_0	N^*
S1	No structures	-	3	5.23×10^{-4}	0.06
S2	Chains	1.7	10	5.23×10^{-4}	2.1
S3	Chains	2.6	10	1.05×10^{-3}	2.9
S4	Chains	3.2	11	5.23×10^{-4}	3.4
S5	Chains	4.7	10	2.62×10^{-3}	4.6
S6	Chains	6.8	10	5.23×10^{-3}	6.5
S7	Bundles of chains	25	12	10^{-2}	24

Table 3. Comparison of simulation results reported in Table 2 (simulations S1 to S7) and the different theories discussed in the text for the average length of chains in the direction of the applied field (in units of number of particles). Predictions of the different theories are evaluated using the data in Table 2. In the case of our theory we have employed Equation (6) and (9), for the De Gennes-Pincus theory we employed Equation (19), for the Zubarev-Iskakova theory we employed Equation (20) and (21) and for the modified Zubarev-Iskakova theory we employed Equation (20) and (30). Unphysical results were shown in bold.

	S1	S2	S3	S4	S5	S6	S7
Simulations $< l >_{\mathrm{sim}}$	No chains	1.7	2.6	3.2	4.7	6.8	25
Our mean-field theory	No chains	2.1	2.9	3.4	4.6	6.5	24
De Gennes-Pincus Theory	No chains	1.4	2.6	3.2	**-1.9**	**-0.5**	**-0.2**
Zubarev-Iskakova Theory	No chains	1.1	1.2	1.3	1.5	1.8	4.4
Modified Zubarev-Iskakova	1.01	2.1	2.8	3.0	4.0	5.4	17

((**For Essays, Feature Articles, Progress Reports, and Reviews,** please insert up to three author biographies and photographs here, max. 100 words each))

Author Photograph(s) ((40 mm broad, 50 mm high, gray scale))

Jordi Faraudo is a tenured scientist at the Institut de Ciència de Materials de Barcelona (ICMAB-CSIC) from 2007. His research interests are in the field of theory and simulation of soft matter, with particular emphasis on self-assembly problems such as supramolecular self-assembly in bulk (vesicles, liposomes,…) or self-assembly at surfaces (organic molecules at metal surfaces) and self-assembly of nano and colloidal particles. He is also interested in fundamental aspects of forces emerging at the nano and colloidal scale such as hydration forces, the hydrophobic effect or ionic forces beyond classical DLVO theory.

Carles Calero received his B.Sc. in Physics at the Universitat de Barcelona and a Ph. D. in theoretical nano magnetism at the City University of New York. He has been a postdoctoral fellow at the Institut de Ciencia de Materials de Barcelona (ICMAB-CSIC), Universitat Politecnica de Catalunya (UPC) and the Center for Polymer Studies at Boston University (CPS, BU). He is currently working at the Universitat de Barcelona in the understanding and modeling of the static and dynamical properties of nanoparticle self-assembly and aggregation, as well as in the study of hydrated biological interfaces.

Juan Camacho is Associate Professor at the Physics Department, Universitat Autònoma de Barcelona from 1995. His current research interests are in the fields of complexity and statistical physics. In particular, he is interested in biological systems, and statistical physics of magnetic dispersions, including foundations and applications.

Table of contents entry

Predicting the self-assembly of superparamagnetic colloids under magnetic fields

J. Faraudo, J.S. Andreu, C. Calero and J. Camacho*

Recent theoretical advances allow quantitative predictions of self-assembly of superparamagnetic colloids under magnetic fields. This Feature Article describes how to employ self-assembly thermodynamics to predict the possible assembled structures from the properties of the colloidal suspension (particle, size, magnetization, concentration, temperature). Quantitative prediction of kinetics is also discussed for the cases in which equilibrium theory is not relevant.

ToC figure ((Please choose one size: 55 mm broad × 50 mm high **or** 110 mm broad × 20 mm high. Please do not use any other dimensions))

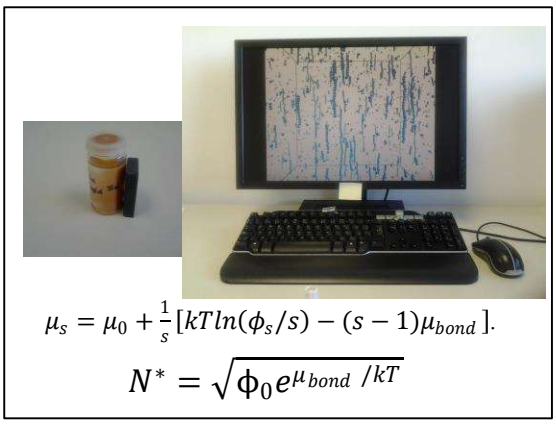

((Supporting Information can be included here using this template))

Supporting Information

Predicting the self-assembly of superparamagnetic colloids under magnetic fields

Jordi Faraudo, Jordi Andreu, Carles Calero and Juan Camacho*

1. Supporting information to magnetic energy calculations

1.1 Addition of a magnetic colloid to a very long chain of magnetic colloids

As in the main text (Section 5.3), we consider the addition of a colloid to a chain of colloids in a tip to tip (or "head to tail") configuration. We assume, as in Section 5.3, all colloids in close contact forming a chain perfectly aligned with the magnetic field (θ=0 as defined in Figure 8). The energy change due to the addition of a colloid to an infinitely long chain can be computed by adding the interaction energy given by Equation (3) between the "new" colloid with all colloids of the chain, located at positions *r=d,2d,3d,…* This gives the convergent series:

$$U_m = -\sum_{n=1}^{\infty} \frac{\mu_0 m_s^2}{2\pi(nd)^3} = -U^* \sum_{n=1}^{\infty} \frac{1}{n^3} = -U^* \cdot \zeta(3) \cong -1.2 \cdot U^*, \qquad (32)$$

where we used that $\zeta(3) = \sum_{n=1}^{\infty} \frac{1}{n^3} = 1.2020569\ldots$ is Apéry's constant and ζ(s) is the Riemann zeta function[63]. This asymptotic limit is clear in Figure 9a. In fact, for chains larger than 10 colloids, the magnetic energy has reached this asymptotic limit for all practical purposes.

The derivation of Equation (32) neglects the induced dipole contribution that could be relevant for weak fields. In the case of weak fields (magnetic response described by linear susceptibility, $\rho_p M(H) = \chi H$), the procedure is very similar, but one has to take into account that the magnetic moment of the colloid is modified by the presence of the chain of colloids.

First of all, let us consider a dimer of two aligned magnetic colloids in contact. The total field *H* sensed by one of the colloids is $H=H_0+H_1$ where H_0 is the externally applied field and H_1 is the field generated by the dipole of one particle over the center of the other particle, which is given by $\mathrm{H_1} = \frac{\mathrm{m(H)}}{2\pi d^3}$. Using Equation (1) we have:

$$\mathrm{H_1} = \frac{\mathrm{m(H)}}{2\pi d^3} = \frac{1}{12}\rho_\mathrm{p}\mathrm{M(H)} = \frac{1}{12}\chi\mathrm{H} \tag{33}$$

Therefore, for a chain of two particles we have:

$$\mathrm{H} = \mathrm{H_0} + \mathrm{H_1} = \mathrm{H_0} + \frac{\mathrm{H_0}}{\frac{12}{\chi}-1} = \frac{\mathrm{H_0}}{1-\frac{\chi}{12}} \tag{34}$$

$$\rho_\mathrm{p}\mathrm{M(H)} = \chi\mathrm{H} = \frac{\chi}{1-\frac{\chi}{12}}\,\mathrm{H_0}\ , \tag{35}$$

which corresponds to equation (5) in the main text. Now let us consider the head-to-tail addition of a colloid to a very long chain. Taking into account Equation (32), we see that the magnetic field sensed by the new colloid of the chain is given by:

$$\mathrm{H} = \mathrm{H_0} + \zeta(3)\cdot\mathrm{H_1} \tag{36}$$

The magnetization of the new colloid of the chain will be given by:

$$\rho_\mathrm{p}\mathrm{M(H)} = \chi\mathrm{H} = \frac{\chi}{1-\zeta(3)\frac{\chi}{6}}\mathrm{H_0} \cong \frac{\chi}{1-\frac{\chi}{5}}\mathrm{H_0} \tag{37}$$

According to Equation (37), the increment in the magnetization due to the induced dipole is about a 20% for $\chi\approx1$ as compared with the magnetization expected without accounting for the induced dipole (χH_0).

1.2 **Addition of a chain to a bundle of two chains**

In Figure 12, we report the conditions under the addition of a third chain to a bundle of two chains produces a bundle of three chains (lateral aggregation) or a bundle with two chains by increasing the length of one of the original chains of the bundle. This figure was derived by doing a systematic comparison of the magnetic energy change involved in the addition of the third chain to a bundle in the two configurations. We illustrate here these calculations in **Figure S1**, reporting two different cases. The first case corresponds to the addition of a chain

of arbitrary length to a bundle of two identical chains with N=15 colloids. In this case, head-to-tail aggregation always produces a larger decrease in the magnetic energy. We show also the calculations for N=30. In this case, there is a crossover at a size of 12 colloids for the incoming, third chain. For chains shorted than this value, lateral aggregation is energetically preferred. However, for incoming chains larger than this value of 12 colloids, lateral aggregation will be preferred. The values reported as dots in Figure 12 of the main paper correspond to crossover values obtained as in Figure S1b.

2. **Supporting information to MagChain Simulations**

Here we provide further details to the MagChain kinetic calculations discussed in Section 4.4 in the main text. In particular, all additional details refer to the previously unpublished results concerning the second example reported in Section 4.4.

The first technical aspect to take into account is that the original MagChain code was written assuming that magnetic particles are at magnetic saturation[36]. This is not an essential feature of the code, and its current version is adapted to deal with the full magnetization curve. The code can consider three different regimes: (a) magnetic saturation (as described in the original article[36]), (b) weak fields (so the susceptibility χ needs to be supplied) or (c) full magnetization curve M=M(H), described by a Langevin function of the form: $M(H) = M_S[\coth(aH) - 1/aH]$ (the parameters of the function can be easily fitted to the magnetic characterization data). Other functions to describe M=M(H) can be easily implemented in the code by the user or by the developers under request. The magnetization curve is employed in the MagChain calculation in the precalculation of the radius of attraction of chains (and therefore in magnetic energy calculations), see Figure 5 in the main text. The magnitude actually employed in the simulations is the radius of attraction of chains of different sizes. In the cases (b) and (c), the calculation of the radius of attraction is made in a way totally analogous to that reported in Ref[36] for the case of magnetic saturation. In the case of a chain

with *s* colloids, the radius of attraction $r_a(s)$ is determined by the distance, in the z axis (defined as the axis of the external magnetic field) at which the attractive magnetic energy is equal to the thermal energy (in absolute value). Therefore, it is the solution of the following equation (see Ref[36]):

$$U_m(\mathrm{r}=\mathrm{r_a}) = -U^* \sum_{n=1}^{\mathrm{s}} \frac{1}{\left[\frac{2\mathrm{r_a}}{\mathrm{d}}+\mathrm{n}-\frac{1}{2}\right]^3} = -\mathrm{k_B T}, \tag{38}$$

where U^* is related to the magnetic moment $m=m(H)$ by Equation (4) in the main paper. The only difference in the case of (b) and (c) with respect to the case (a) of magnetic saturation is that the solution of Equation (38) requires first the determination of the magnetic moment of the particles, $m=m(H)$. For a chain of *s* particles, this is done using an iterative method, an approach which is standard in magnetic calculations.

Concerning the details of the MagChain simulation reported in Figure 7, we first computed the radius of attraction employing a Langevin function fit to the experimental $M=M(H)$ curve reported in Figure 1 and considering an external magnetic field of 30 mT. The results for the radius of attraction are shown in Figure S2. As seen in Figure S2, for large chains the size of the attraction region approaches $2r_a \approx 2.79d$ (recall that d=170 nm is the diameter of a colloid). Once the attraction radius are computed, we performed the MagChain simulation employing an initial random distribution of 5000 colloids inside a simulation box of size 369.25*d* in both the x and y directions and 738.5*d* in the z direction (the direction of the magnetic field). In this way we obtain a volume fraction of 2.6×10^{-5} as employed in experiments, as discussed in Section 4.4. The employed time step was $0.01\cdot d^2/D_0 \approx 1.12\times10^{-4}$ s (D_0=2.57×10^{-12} m^2/s is the diffusion coefficient of a single colloid).

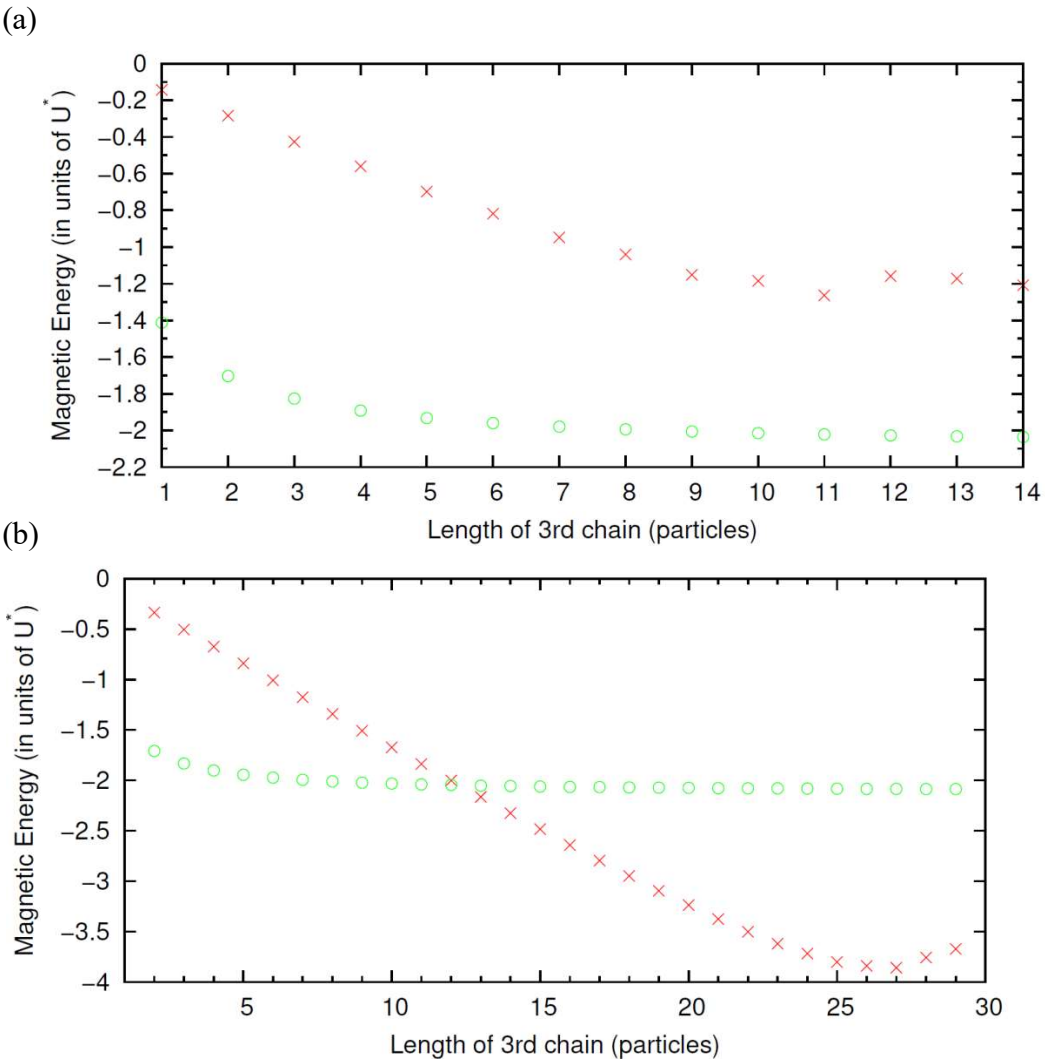

Figure S1. Magnetic energy change due to the addition of a third chain of arbitrary lenght to a bundle of two identical chains with *N* colloids, with *N*=15 in (a) and *N*=30 in (b). The circles correspond to head-to-tail aggregation of the third chain and the crosses correspond to lateral aggregation, giving rise to a bundle with three chains.

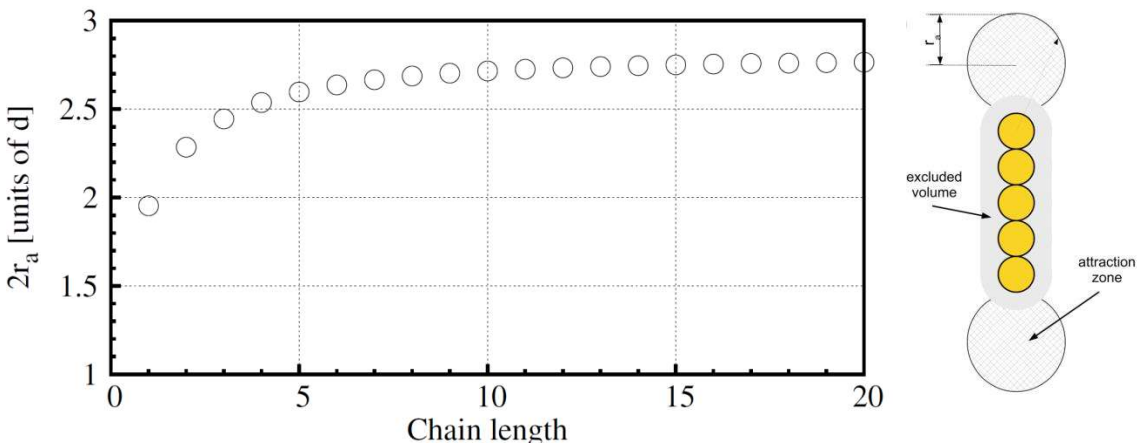

Figure S2. Size of the attraction region located at the head and tail of a chain of magnetic colloids as a function of the chain length calculated for the particles shown in Figure 1b under a magnetic field of 30 mT. Right: scheme indicating the location of the attraction zones of radius r_a.

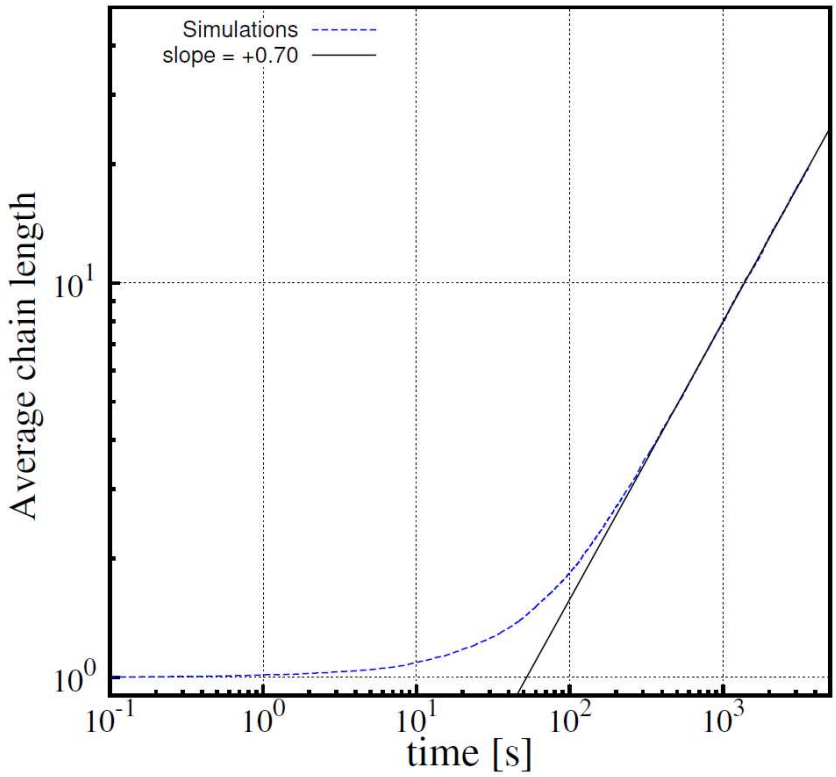

Figure S3. Logarithmic plot of the average length of chains shown in Figure 7 in the main paper together with a fit to a power law of the form t^z with an exponent z=0.7.